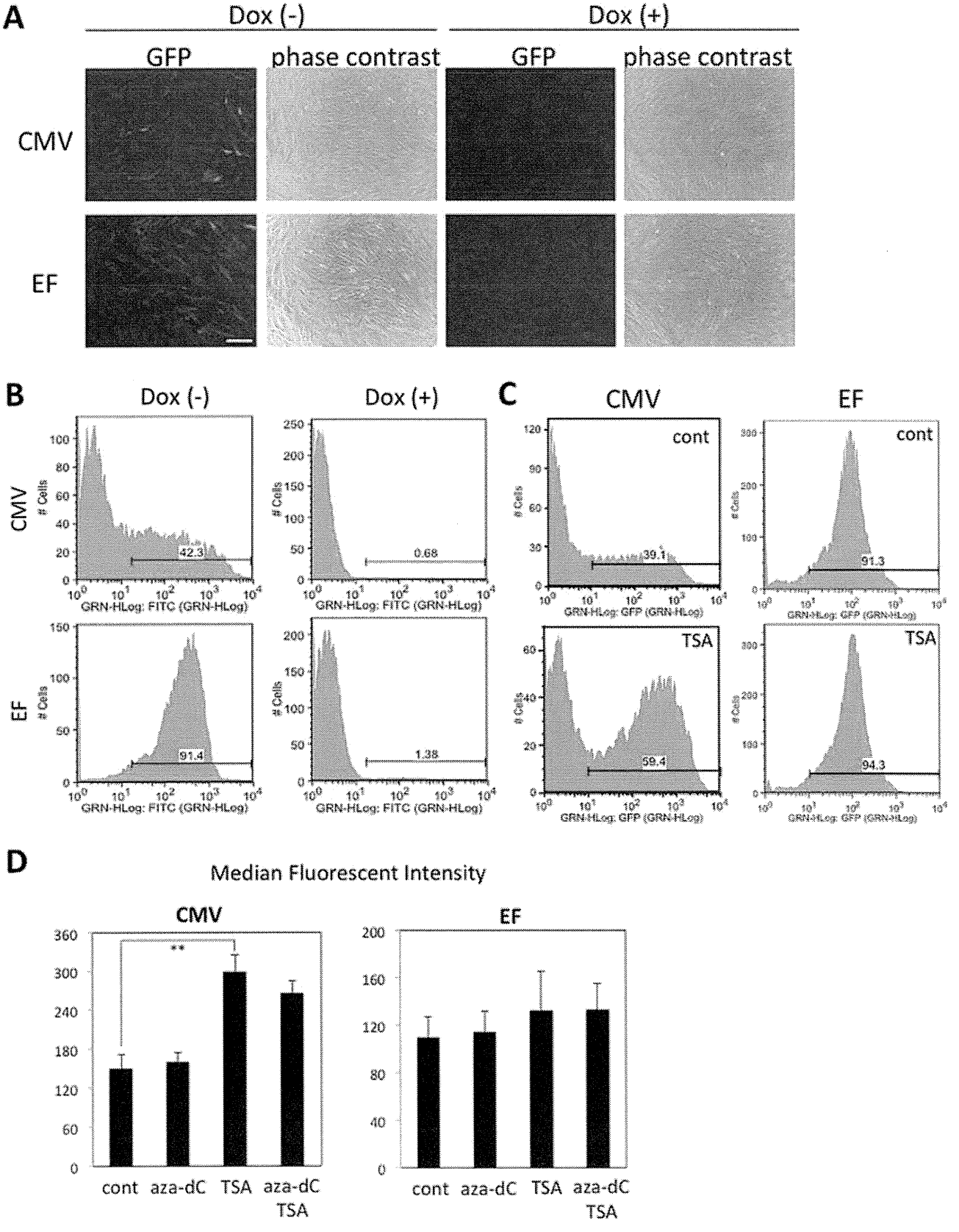

Figure 3. Blasticidin selection of hADMPCs transduced with single tet-off lentiviral vector platform. hADMPCs were transduced with pTRE-EGFP-CMV-tTA-2A-Bsd (CMV) or pTRE-EGFP-EF-tTA-2A-Bsd (EF) at m.o.i. of 250. The cells were treated with 4 μg/mL blasticidin and 1 μg/mL Dox for 2 weeks. Then, the cells were cultured in the absence (Dox (-)) or presence (Dox (+)) of 1 μg/mL Dox for 4 days, and analyzed under a microscope (A) and flow cytometer (B). The cells were treated with 100 nM TSA (TSA), 5 μM 5-aza-dC (aza-dC), or both for 48 h before analyzed by flow

cytometer. (C) A representative fluorescence histogram of EGFP. (D) The median fluorescence intensities of the EGFP-expressing populations. Error bars represent the standard error of 3 independent analyses. **, P<0.01 (Student's t test). Scale bar, 200 μm.
doi:10.1371/journal.pone.0066274.g003

C-terminus (tTA-2A) and Bsd. tTA-2A binds to the TRE-tight in the absence of Dox, a tet derivative, and activates transcription of EGFP to a very high level. In the presence of Dox, tTA-2A is unable to bind the TRE-Tight in a tet-responsive promoter, and the system is inactive.

To investigate the usefulness of these lentiviral vectors, hADMPCs were transduced with pTRE-EGFP-CMV-tTA-2A-Bsd or pTRE-EGFP-EF-tTA-2A-Bsd at a m.o.i. of 250. As shown in Figure 2C, expression of EGFP was observed in the absence of Dox, whereas addition of Dox (1 μg/mL) was enough to suppress the expression. Flow cytometry analysis revealed that the transduction efficiency was relatively low (EGFP-positive cells were 7.5~10%) compared with that of CSII-CMV-EGFP or CSII-EF-EGFP (EGFP-positive cells were 45% or 77% at a m.o.i. of 250, respectively; Figure 1A), and the tet-off system completely abolished gene expression in the presence of Dox (Figure 2D). Flow cytometry analysis also revealed that fluorescent intensity was relatively uniform in hADMPCs transduced with pTRE-EGFP-EF-tTA-2A-Bsd, but a wide range of fluorescent intensities was observed in hADMPCs infected with pTRE-EGFP-CMV-tTA-2A-Bsd. These data suggest that tTA-2A functions properly in this system. Moreover, western blot analysis against tTA showed the efficient cleavage (>95%) of tTA-2A-Bsd proteins into tTA-2A and Bsd (Figure 2E).

To further determine that Bsd cleaved from tTA-2A-Bsd was effective in this system, 4 μg/mL blasticidin was administered to hADMPCs. Within 1 week after the selection, control hADMPCs were completely killed (data not shown), whereas hADMPCs that were successfully transduced with either pTRE-EGFP-CMV-tTA-2A-Bsd or pTRE-EGFP-EF-tTA-2A-Bsd could survive and proliferate, demonstrating that Bsd from tTA-2A-Bsd is sufficient to confer blasticidin resistance to the cells. The surviving cells were kept in culture medium with blasticidin and then divided into 2 populations, either with Dox (1 μg/mL) or without Dox. As shown in Figure 3A and 3B, almost all (>90%) the cells transduced with pTRE-EGFP-EF-tTA-2A-Bsd strongly expressed EGFP in the absence of Dox. In hADMPCs transduced with pTRE-EGFP-CMV-tTA-2A-Bsd, however, >50% of the cells were EGFP negative regardless of their blasticidin resistance. Moreover, fluorescent intensities were quite variable; some cells expressed very high levels of EGFP, while others expressed very low levels (Figure 3A and 3B). This might be due to "promoter suppression," transcript repression of an upstream transcriptional unit by a downstream unit when 2 transcriptional units lie adjacent in head-to-tail tandem on a chromosome [28,29]. Studies have revealed that the suppression by adjacent units is epigenetic and involves modification of the chromatin structure, including DNA methylation at CpG sites within the promoter, histone deacetylation, histone methylation at specific residues (e.g., H3K9, H3K27), and densely packed nucleosomes that create a closed chromatin structure. In order to determine if inhibiting histone deacetylases or DNA methylation would re-induce EGFP expression, pTRE-EGFP-CMV-tTA-2A-Bsd cells were treated with histone deacetylase inhibitor trichostatin A (TSA) and/or DNA methylation inhibitor 5-aza-2′-deoxycytidine (5-aza-dC). TSA treatment significantly increased the number of EGFP-positive cells and strengthened the fluorescent intensities of EGFP, whereas 5-aza-dC had no effect, suggesting that EGFP expression was repressed by histone deacetylation when stably transduced with pTRE-EGFP-CMV-tTA-2A-Bsd (Figure 3C and 3D). These inhibitors had no effect on hADMPCs transduced with pTRE-EGFP-EF-tTA-2A-Bsd. These data suggest that the dual-promoter lentiviral vector using the EF promoter is more resistant to gene silencing than that using the CMV promoter.

Blasticidin-selected hADMPCs Maintain the Properties of Their Parental hADMPCs

hADMPCs are an attractive material for cell therapy because of their ability to secrete various cytokines and growth factors. These cells also have the ability to differentiate into various types of cells, including adipocytes, chondrocytes, osteocytes, hepatocytes, cardiomyoblasts, and neuronal cells. Gene manipulation of hADMPCs may thus generate great possibilities for cell therapy and tissue engineering. From this point of view, the development of an efficient and stable Dox-responsive gene transfer system to achieve high levels of transgene expression in hADMPCs, without affecting the phenotype, is of special interest for the field. We therefore studied the cell properties of hADMPCs transduced with the single tet-off lentiviral vector after blasticidin selection. Flow cytometry analysis revealed no changes in the expression of the main surface markers (positive for CD13, CD29, CD44, CD73, CD90, CD105, and CD166, and negative for CD34) either in the absence or presence of Dox (Figure 4). To further confirm the properties of hADMPCs, the cells were differentiated into adipocytes, osteocytes, chondrocytes, and neuronal cells. As shown in Figure 5, blasticidin-selected hADMPCs maintained their ability to differentiate into adipocytes, osteocytes, chondrocytes, and neuronal cells. Moreover, EGFP was stably expressed in the differentiated cells only in the absence of Dox (Figure 5).

Discussion

In recent years, there is growing interest in the use of MSCs for cell therapy and tissue engineering because of their differentiation potential and ability to secrete growth factors [7–11]. Furthermore, because of their hypo-immunogenicity and immune modulatory effects, MSCs are good candidates for gene delivery vehicles for therapeutic purposes [12,14]. In addition to primary MSCs, genetically modified MSCs have been applied to bone regeneration, muscle repair, diabetes, Parkinson's disease, and myocardial infarction recovery [14,30–35]. Duan et al. reported that the angiogenic effect of MSCs could be enhanced by adenovirus-mediated HGF overexpression in the treatment of cardiac ischemia injury [14]. Karnieli et al. and Li et al. both reported the reversal of hyperglycemia in streptozotocin-induced diabetic mice after transplantation of insulin-producing cells originating from genetically modified Pdx-1 expressing MSCs [32,33].

While significant progress has been made in the use of genetically modified MSCs for basic and applied research, the current methods for gene manipulation are still insufficient for some applications. Adenoviral vectors are commonly used for transient expression because they remain epichromosomal in the host cells, and their ability to transiently infect target cells minimizes the risk of insertional mutagenesis [36]. However, relatively brief transgene expression may limit the utility of this approach to tissue repair applications. On the other hand, lentiviral vectors, which are promising vectors for gene delivery in primary human cells, integrate into the host cell genome, which may be an appropriate strategy for tissue repair applications

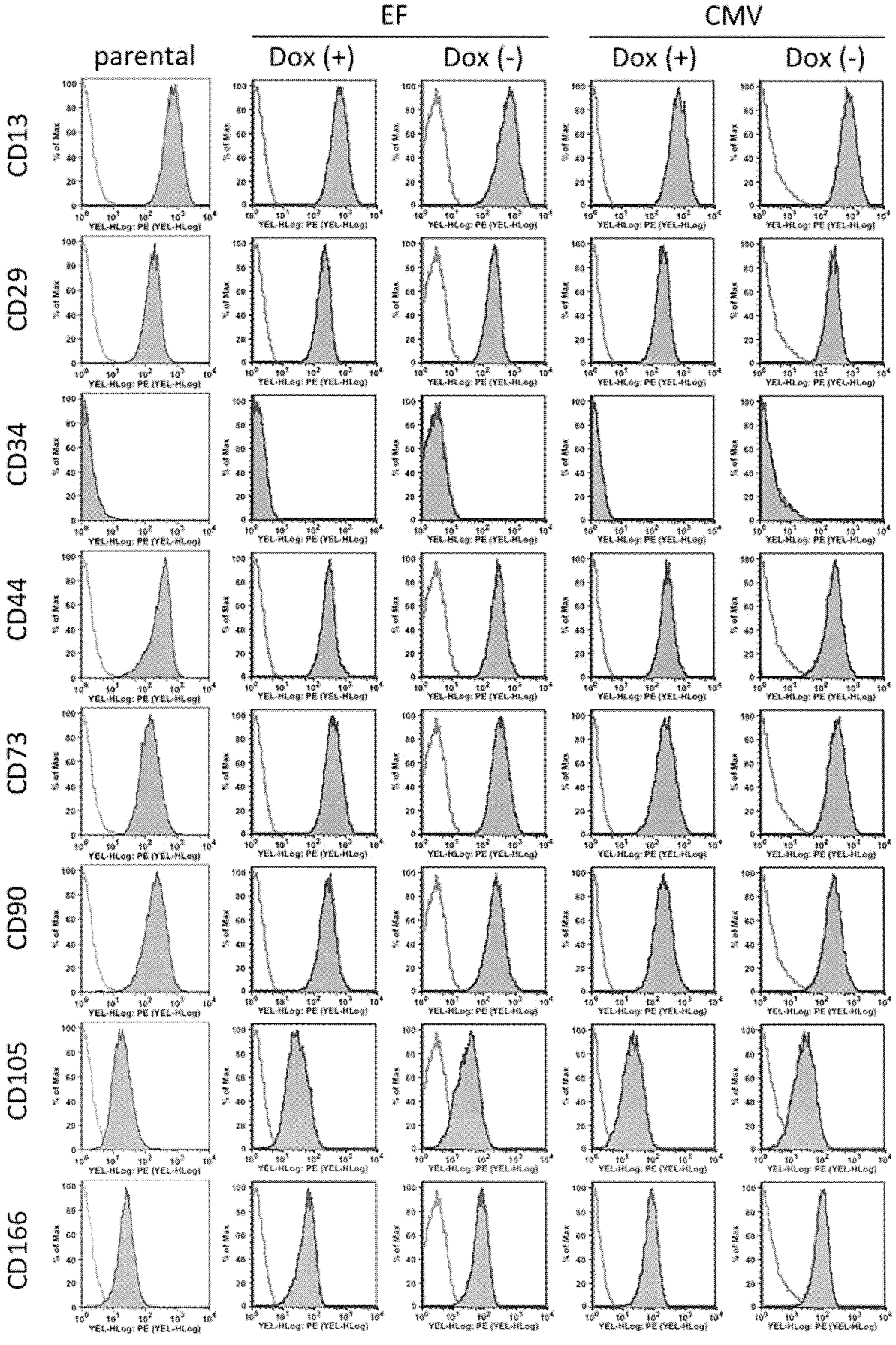
EF
CMV
parental
Dox (+)
Dox (-)
Dox (+)
Dox (-)
CD13
CD29
CD34
CD44
CD73
CD90
CD105
CD166
% of Max
YEL-HLog: PE (YEL-HLog)

Figure 4. Expression pattern of surface cell markers on Dox-responsive hADMPCs. Dox-responsive hADMPCs after selection by blasticidin were cultured in the absence (Dox(-)) or presence (Dox (+)) of 1 μg/mL Dox for 4 days. Expression of the different surface markers were analyzed by flow cytometry and compared to the expression by a parental hADMPCs. They were stained with PE-coupled antibodies against CD13, CD29, CD34, CD44, CD73, CD90, CD105, and CD166. Histogram of a PE-coupled mouse IgG1 κ isotype control is shown in gray. CMV; hADMPCs transduced with pTRE-EGFP-CMV-tTA-2A-Bsd, EF; hADMPCs transduced with pTRE-EGFP-EF-tTA-2A-Bsd.
doi:10.1371/journal.pone.0066274.g004

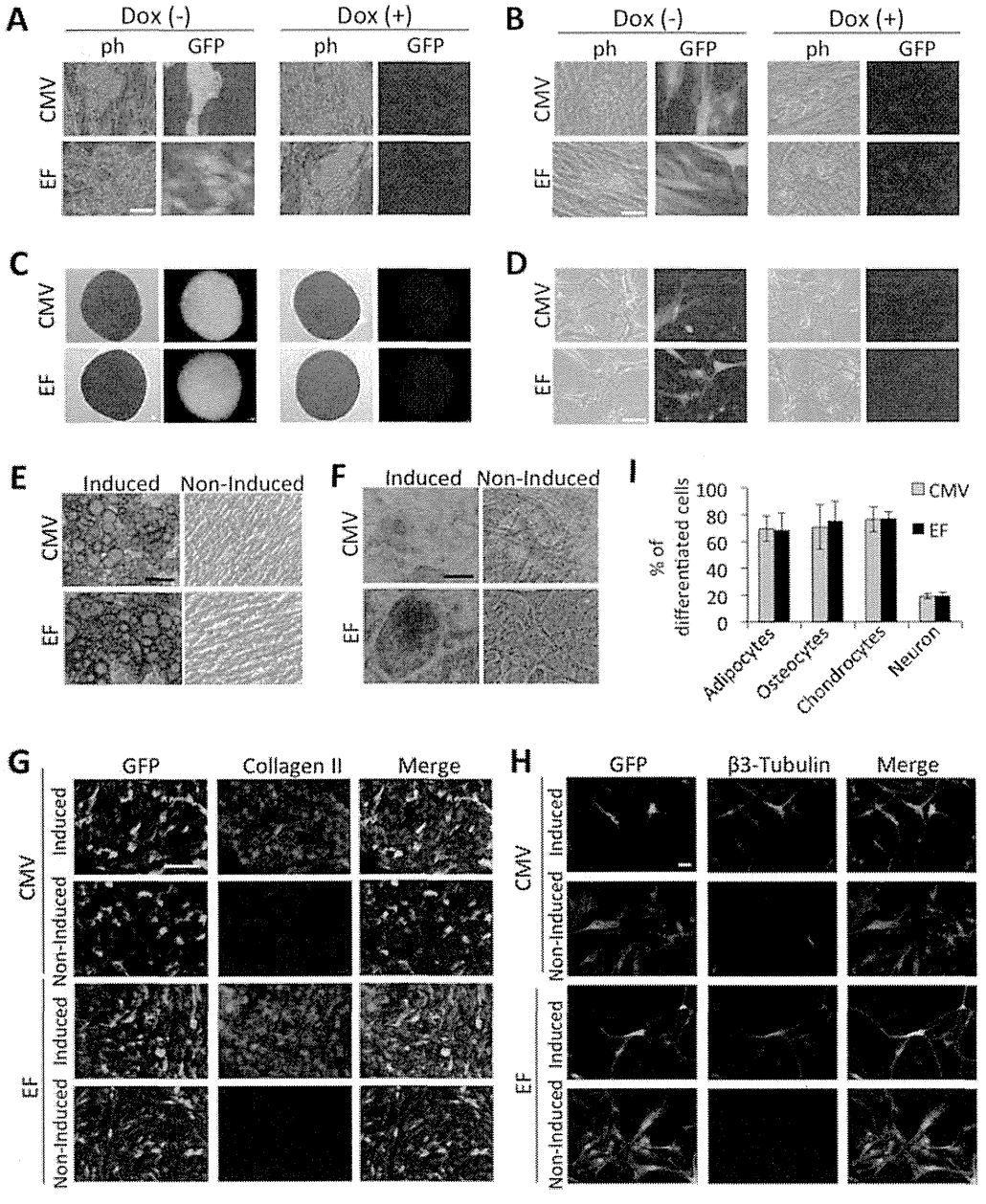

Figure 5. Differentiation potential of Dox-responsive hADMPCs. Dox-responsive hADMPCs were differentiated into adipocytes (A, E), osteocytes (B, F), chondrocytes (C, G), and neuronal cells (D, H). (A–D) Phase contrast (ph) and fluorescent (GFP) images. Dox-responsive hADMPCs were differentiated in the absence of Dox (Dox(−)) or in the presence of 1 μg/mL Dox (Dox(+)) as described in the material and methods section. (E–I) Confirmation of differentiated cells by oil red O staining for adipocytes (E), alizarin red staining for osteocytes (F), immunohistochemical staining against collagen II for chondrocytes (G), and immunohistochemical staining against β3-tubulin for neuronal cells (H). The percentages of differentiated cells to each cell type were calculated by the computerized image analysis (I). Cells that were not induced to differentiate (non-induced) were used as a negative control. CMV; hADMPCs transduced with pTRE-EGFP-CMV-tTA-2A-Bsd, EF; hADMPCs transduced with pTRE-EGFP-EF-tTA-2A-Bsd. Scale bar, 50 μm.
doi:10.1371/journal.pone.0066274.g005

requiring sustained, long-term expression of therapeutic proteins. In this study, we generated novel lentiviral vectors with a tet-off system, and demonstrated that our lentiviral vector systems were significantly effective and strictly regulated in hADMPCs, without affecting their stem cell properties.

Gene silencing is of considerable importance where stable, long-term expression is required. Researchers have reported that transgene silencing occurred when the CMV promoter was used in some cell types, especially in embryonic stem cells [15–17]. Since Kawabata et al. also demonstrated that virus-derived promoters inefficiently functioned in embryonic stem cells in gene transfer experiments [37], down-regulation and unsuitability of promoters in stem cells should be considered. Therefore, transduction efficacy and durability of transgene expression in hADMPCs is also an important issue to be determined. Qin et al. reported that the human EF-1α promoter and the TRE promoter are more efficient than the CMV promoter to drive lentiviral mediated transgene expression in rat bone marrow-derived MSCs [18]. McGinley et al. also showed that EF-1α and human phosphoglycerate kinase-1 (PGK) promoters have a clear advantage over the CMV promoter in transducing rat bone marrow-derived MSC transduction with lentivirus [19]. Consistent with their findings, our data also demonstrated that the EF-1α promoter was more efficient than the CMV promoter to drive EGFP expression in hADMPCs (Figure 1A, B). Moreover, a significant decrease in fluorescent intensity was observed by 28 days after transduction with lentiviral vector CSII-CMV-EGFP (Figure 1C), suggesting that the CMV promoter might be silenced in hADMPCs. We also demonstrated the intriguing finding that most (>90%) of the hADMPCs transduced with pTRE-EGFP-EF-tTA-2A-Bsd strongly expressed EGFP in the absence of Dox, whereas >50% of the cells transduced with pTRE-EGFP-CMV-tTA-2A-Bsd were EGFP negative, regardless of their blasticidin resistance (Figure 3A, B). Our data demonstrated that the inhibitor of histone deacetylation trichostatin A (TSA) re-induced the expression of EGFP (Figure 3C, D), suggesting that "promoter suppression" might occur by histone deacetylation, not by DNA methylation of CpG sites within the TRE tight promoter. "Promoter suppression" is a transcript repression of a 5′ transcriptional unit by a 3′ unit when 2 transcriptional units lie adjacent in head-to-tail tandem on a chromosome [28,29]. In this study, it is possible that the downstream unit of CMV-tTA-2A-Bsd repressed the upstream unit of TRE-EGFP because (1) resistance to blasticidin implies the transcriptional unit of CMV-tTA-2A-Bsd is active, and (2) reactivation of EGFP expression by TSA implies the transcriptional unit of TRE-EGFP is epigenetically silenced. In order to eliminate the promoter suppression or transcriptional interference between 2 transcriptional units, some researchers have been trying to separate the 2 units by polyadenylation, terminator, and insulator sequences [28,38]. However, these sequences extend the lentiviral vector size, which may affect the lentiviral titers produced from the vector. From this point of view, our finding that the transcriptional unit driven from the TRE tight promoter is resistant to gene silencing when arranged in tandem with the EF-tTA-2A-Bsd transcriptional unit (Figure 3) is of interest in the fields of both basic and clinical research, although the underlying mechanism remains elusive.

In general, large numbers of cells displaying the appropriate phenotypes are required for tissue engineering. Moreover, fully differentiated cells do not proliferate [39]. Therefore, in order to obtain enough cells to perform a transplant from genetically modified MSCs, it is important to develop a system in which the gene of interest is tightly regulated and inducible, and in which stably expressing transgenic cell lines can be obtained without affecting their stem cell properties. Using the system, MSCs transduced with lentiviral vectors can be selected and increased in numbers from a limited number of MSCs, before the target genes are induced. After obtaining an adequate number of gene-manipulated MSCs, the target genes could be induced in order to start differentiation. According to our data, hADMPCs transduced with pTRE-EGFP-EF-tTA-2A-Bsd were successfully selected by blasticidin, could proliferate, maintain their stem cell properties, and regulate EGFP expression tightly by Dox (Figure 4, 5), demonstrating that this all-in-one lentiviral vector is a promising gene delivery system for generating the material for artificial organs.

A major advantage of using the 2A cleavage factor in the construction of multi-cistronic vectors is its small size compared to internal promoter entry site (IRES) sequences. Because the titer of the lentivirus decreases with increasing size of the lentiviral vector, it is important to minimize the length of the sequences. In addition, linkage of 2 genes by 2A peptide resulted in efficient co-expression of the genes, whereas a gene placed downstream of an IRES is expressed at 2- to 3-fold lower levels than a gene placed upstream [40,41]. In this study, tTA-2A-Bsd cassette driven from CMV or EF-1α promoter showed ~90% cleavage (Figure 3). However, the point that should be considered is the effect of residual 2A peptide on the protein. As the processing occurred at the end of the 2A peptide, the 2A tag remains attached at the tTA C-terminus. Our data demonstrated that the presence of this extra 2A peptide did not seem to interfere with the activity of tTA since Dox strictly regulated the expression of EGFP under the control of TRE-tight promoter (Figure 2D, 3A, 3B and 5). Moreover, when Bsd is cleaved, an additional proline is attached at the N-terminus. We demonstrated that this did not affect a function of Bsd because hADMPCs transduced with either pTRE-EGFP-CMV-tTA-2A-Bsd or pTRE-EGFP-EF-tTA-2A-Bsd could survive and proliferate in medium containing blasticidin at a concentration at which all of the parental hADMPCs died.

Another advantage of our lentiviral system is the availability of a restriction enzyme treatment/ligation independent cloning system, called the Gateway system (Invitrogen). In general, the construction of lentiviral vectors using a conventional restriction enzyme/ligation cloning method has poor efficiency due to the large sizes and the lack of proper cloning sites. In our hands, cloning efficiency into our new lentiviral vectors pTRE-RfA-CMV-tTA-2A-Bsd or pTRE-RfA-EF-tTA-2A-Bsd using LR recombination reaches nearly 100%, saving time and effort in construction of the vectors. In addition, there are several resources available that take advantage of the Gateway vector. For example, CCSB Human ORFeome Collection (Dana-Farber Cancer Institute, Center for Cancer Systems Biology) represents almost 12,000 fully-sequenced cloned human ORFs which can be readily transferred to Gateway compatible destination vectors for various functional proteomics studies [42]. Block-iT pol II miR RNAi system from Invitrogen, which is designed to express artificial miRNAs, also enables compatibility with Gateway destination vectors for gene knock-down experiments [43].

In conclusion, our new single tet-off lentiviral vector system provides powerful tools not only for applied research on hADMPCs and other stem cells, but also basic research on a variety of cell lines and primary cells.

Acknowledgments

We thank J. Uda, S. Tamura, C. Sone, K. Nakagita, and H. Isshi for technical support. We thank Dr. Tyler Jacks for providing the pSico plasmid and Dr. Hiroyuki Miyoshi for the CSII-EF-RfA, CSII-CMV-RfA, pCMV-VSVG-RSV-Rev, and pCAG-HIVg/p plasmids.

Author Contributions

Conceived and designed the experiments: HM MM. Performed the experiments: HM MM KS HO AM. Analyzed the data: HM MM KS. Contributed reagents/materials/analysis tools: HM MM HO AI AM. Wrote the paper: HM MM TH.

References

1. Okura H, Komoda H, Saga A, Kakuta-Yamamoto A, Hamada Y, et al. (2010) Properties of hepatocyte-like cell clusters from human adipose tissue-derived mesenchymal stem cells. Tissue engineering Part C, Methods 16: 761–770.
2. Okura H, Matsuyama A, Lee CM, Saga A, Kakuta-Yamamoto A, et al. (2010) Cardiomyoblast-like cells differentiated from human adipose tissue-derived mesenchymal stem cells improve left ventricular dysfunction and survival in a rat myocardial infarction model. Tissue engineering Part C, Methods 16: 417–425.
3. Okura H, Komoda H, Fumimoto Y, Lee CM, Nishida T, et al. (2009) Transdifferentiation of human adipose tissue-derived stromal cells into insulin-producing clusters. Journal of artificial organs : the official journal of the Japanese Society for Artificial Organs 12: 123–130.
4. Safford KM, Safford SD, Gimble JM, Shetty AK, Rice HE (2004) Characterization of neuronal/glial differentiation of murine adipose-derived adult stromal cells. Experimental neurology 187: 319–328.
5. Leu S, Lin YC, Yuen CM, Yen CH, Kao YH, et al. (2010) Adipose-derived mesenchymal stem cells markedly attenuate brain infarct size and improve neurological function in rats. Journal of translational medicine 8: 63.
6. Ikegame Y, Yamashita K, Hayashi S, Mizuno H, Tawada M, et al. (2011) Comparison of mesenchymal stem cells from adipose tissue and bone marrow for ischemic stroke therapy. Cytotherapy 13: 675–685.
7. Tan B, Luan Z, Wei X, He Y, Wei G, et al. (2011) AMP-activated kinase mediates adipose stem cell-stimulated neuritogenesis of PC12 cells. Neuroscience 181: 40–47.
8. Reid AJ, Sun M, Wiberg M, Downes S, Terenghi G, et al. (2011) Nerve repair with adipose-derived stem cells protects dorsal root ganglia neurons from apoptosis. Neuroscience.
9. Rehman J, Traktuev D, Li J, Merfeld-Clauss S, Temm-Grove CJ, et al. (2004) Secretion of angiogenic and antiapoptotic factors by human adipose stromal cells. Circulation 109: 1292–1298.
10. Lee EY, Xia Y, Kim WS, Kim MH, Kim TH, et al. (2009) Hypoxia-enhanced wound-healing function of adipose-derived stem cells: increase in stem cell proliferation and up-regulation of VEGF and bFGF. Wound repair and regeneration : official publication of the Wound Healing Society [and] the European Tissue Repair Society 17: 540–547.
11. Moriyama M, Moriyama H, Ueda A, Nishibata Y, Okura H, et al. (2012) Human adipose tissue-derived multilineage progenitor cells exposed to oxidative stress induce neurite outgrowth in PC12 cells through p38 MAPK signaling. BMC Cell Biol 13: 21.
12. Wu H, Ye Z, Mahato RI (2011) Genetically modified mesenchymal stem cells for improved islet transplantation. Mol Pharm 8: 1458–1470.
13. Pfeifer A, Ikawa M, Dayn Y, Verma IM (2002) Transgenesis by lentiviral vectors: lack of gene silencing in mammalian embryonic stem cells and preimplantation embryos. Proc Natl Acad Sci U S A 99: 2140–2145.
14. Duan HF, Wu CT, Wu DL, Lu Y, Liu HJ, et al. (2003) Treatment of myocardial ischemia with bone marrow-derived mesenchymal stem cells overexpressing hepatocyte growth factor. Mol Ther 8: 467–474.
15. Brooks AR, Harkins RN, Wang P, Qian HS, Liu P, et al. (2004) Transcriptional silencing is associated with extensive methylation of the CMV promoter following adenoviral gene delivery to muscle. J Gene Med 6: 395–404.
16. Kim S, Kim GJ, Miyoshi H, Moon SH, Ahn SE, et al. (2007) Efficiency of the elongation factor-1alpha promoter in mammalian embryonic stem cells using lentiviral gene delivery systems. Stem Cells Dev 16: 537–545.
17. Meilinger D, Fellinger K, Bultmann S, Rothbauer U, Bonapace IM, et al. (2009) Np95 interacts with de novo DNA methyltransferases, Dnmt3a and Dnmt3b, and mediates epigenetic silencing of the viral CMV promoter in embryonic stem cells. EMBO Rep 10: 1259–1264.
18. Qin JY, Zhang L, Clift KL, Hulur I, Xiang AP, et al. (2010) Systematic comparison of constitutive promoters and the doxycycline-inducible promoter. PLoS One 5: e10611.
19. McGinley L, McMahon J, Strappe P, Barry F, Murphy M, et al. (2011) Lentiviral vector mediated modification of mesenchymal stem cells & enhanced survival in an in vitro model of ischaemia. Stem Cell Res Ther 2: 12.
20. Weber W, Fussenegger M (2006) Pharmacologic transgene control systems for gene therapy. J Gene Med 8: 535–556.
21. Shi Q, Tian X, Zhao Y, Luo H, Tian Y, et al. (2011) Anti-arthritic effects of FasL gene transferred intra-articularly by an inducible lentiviral vector containing improved tet-on system. Rheumatol Int.
22. Wiederschain D, Wee S, Chen L, Loo A, Yang G, et al. (2009) Single-vector inducible lentiviral RNAi system for oncology target validation. Cell Cycle 8: 498–504.
23. Hioki H, Kuramoto E, Konno M, Kameda H, Takahashi Y, et al. (2009) High-level transgene expression in neurons by lentivirus with Tet-Off system. Neurosci Res 63: 149–154.
24. Benabdellah K, Cobo M, Munoz P, Toscano MG, Martin F (2011) Development of an all-in-one lentiviral vector system based on the original TetR for the easy generation of Tet-ON cell lines. PLoS One 6: e23734.
25. Okura H, Saga A, Fumimoto Y, Soeda M, Moriyama M, et al. (2011) Transplantation of human adipose tissue-derived multilineage progenitor cells reduces serum cholesterol in hyperlipidemic Watanabe rabbits. Tissue engineering Part C, Methods 17: 145–154.
26. Saga A, Okura H, Soeda M, Tani J, Fumimoto Y, et al. (2011) HMG-CoA reductase inhibitor augments the serum total cholesterol-lowering effect of human adipose tissue-derived multilineage progenitor cells in hyperlipidemic homozygous Watanabe rabbits. Biochemical and biophysical research communications 412: 50–54.
27. Okura H, Saga A, Fumimoto Y, Soeda M, Moriyama M, et al. (2011) Transplantation of human adipose tissue-derived multilineage progenitor cells reduces serum cholesterol in hyperlipidemic Watanabe rabbits. Tissue Eng Part C Methods 17: 145–154.
28. Villemure JF, Savard N, Belmaaza A (2001) Promoter suppression in cultured mammalian cells can be blocked by the chicken beta-globin chromatin insulator 5′HS4 and matrix/scaffold attachment regions. J Mol Biol 312: 963–974.
29. Emerman M, Temin HM (1986) Comparison of promoter suppression in avian and murine retrovirus vectors. Nucleic Acids Res 14: 9381–9396.
30. Tai K, Pelled G, Sheyn D, Bershteyn A, Han L, et al. (2008) Nanobiomechanics of repair bone regenerated by genetically modified mesenchymal stem cells. Tissue Eng Part A 14: 1709–1720.
31. Goudenege S, Pisani DF, Wdziekonski B, Di Santo JP, Bagnis C, et al. (2009) Enhancement of myogenic and muscle repair capacities of human adipose-derived stem cells with forced expression of MyoD. Mol Ther 17: 1064–1072.
32. Li Y, Zhang R, Qiao H, Zhang H, Wang Y, et al. (2007) Generation of insulin-producing cells from PDX-1 gene-modified human mesenchymal stem cells. J Cell Physiol 211: 36–44.
33. Karnieli O, Izhar-Prato Y, Bulvik S, Efrat S (2007) Generation of insulin-producing cells from human bone marrow mesenchymal stem cells by genetic manipulation. Stem Cells 25: 2837–2844.
34. Dezawa M, Kanno H, Hoshino M, Cho H, Matsumoto N, et al. (2004) Specific induction of neuronal cells from bone marrow stromal cells and application for autologous transplantation. J Clin Invest 113: 1701–1710.
35. Fan L, Lin C, Zhuo S, Chen L, Liu N, et al. (2009) Transplantation with survivin-engineered mesenchymal stem cells results in better prognosis in a rat model of myocardial infarction. Eur J Heart Fail 11: 1023–1030.
36. Ghosh SS, Gopinath P, Ramesh A (2006) Adenoviral vectors: a promising tool for gene therapy. Appl Biochem Biotechnol 133: 9–29.
37. Kawabata K, Sakurai F, Yamaguchi T, Hayakawa T, Mizuguchi H (2005) Efficient gene transfer into mouse embryonic stem cells with adenovirus vectors. Mol Ther 12: 547–554.
38. Tian J, Andreadis ST (2009) Independent and high-level dual-gene expression in adult stem-progenitor cells from a single lentiviral vector. Gene Ther 16: 874–884.
39. Clarke MF, Fuller M (2006) Stem cells and cancer: two faces of eve. Cell 124: 1111–1115.
40. Chinnasamy D, Milsom MD, Shaffer J, Neuenfeldt J, Shaaban AF, et al. (2006) Multicistronic lentiviral vectors containing the FMDV 2A cleavage factor demonstrate robust expression of encoded genes at limiting MOI. Virol J 3: 14.
41. Ibrahimi A, Vande Velde G, Reumers V, Toelen J, Thiry I, et al. (2009) Highly efficient multicistronic lentiviral vectors with peptide 2A sequences. Hum Gene Ther 20: 845–860.
42. Temple G, Gerhard DS, Rasooly R, Feingold EA, Good PJ, et al. (2009) The completion of the Mammalian Gene Collection (MGC). Genome Res 19: 2324–2333.
43. Liang Z, Wu H, Reddy S, Zhu A, Wang S, et al. (2007) Blockade of invasion and metastasis of breast cancer cells via targeting CXCR4 with an artificial microRNA. Biochem Biophys Res Commun 363: 542–546.

International Journal of Cardiology 168 (2013) 261–269

Contents lists available at ScienceDirect

International Journal of Cardiology

journal homepage: www.elsevier.com/locate/ijcard

The use of cell-sheet technique eliminates arrhythmogenicity of skeletal myoblast-based therapy to the heart with enhanced therapeutic effects ☆

Takuya Narita [a], Yasunori Shintani [a], Chiho Ikebe [a], Masahiro Kaneko [a], Narumi Harada [a], Nomathamsanqa Tshuma [a], Kunihiko Takahashi [a], Niall G. Campbell [a], Steven R. Coppen [a], Kenta Yashiro [a], Yoshiki Sawa [b], Ken Suzuki [a,*]

[a] William Harvey Research Institute, Barts and The London School of Medicine and Dentistry, Queen Mary University of London, London, UK
[b] Cardiovascular Surgery, Osaka University, Osaka, Japan

ARTICLE INFO

Article history:
Received 21 December 2011
Received in revised form 16 June 2012
Accepted 15 September 2012
Available online 6 October 2012

Keywords:
Cell-based therapy
Bioengineering technology
Cell-sheet technique
Intramyocardial injection
Ventricular arrhythmia
Heart failure

ABSTRACT

Background: Clinical application of skeletal myoblast transplantation has been curtailed due to arrhythmogenicity and inconsistent therapeutic benefits observed in previous studies. However, these issues may be solved by the use of a new cell-delivery mode. It is now possible to generate "cell-sheets" using temperature-responsive dishes without artificial scaffolds. This study aimed to validate the safety and efficacy of epicardial placement of myoblast-sheets (myoblast-sheet therapy) in treating heart failure.

Methods and results: After coronary artery ligation in rats, the same numbers of syngeneic myoblasts were transplanted by intramyocardial injection or cell-sheet placement. Continuous radio-telemetry monitoring detected increased ventricular arrhythmias, including ventricular tachycardia, after intramyocardial injection compared to the sham-control, while these were abolished in myoblast-sheet therapy. This effect was conjunct with avoidance of islet-like cell-cluster formation that disrupts electrical conduction, and with prevention of increased arrhythmogenic substrates due to exaggerated inflammation. Persistent ectopic donor cells were found in the lung only after intramyocardial injection, strengthening the improved safety of myoblast-sheet therapy. In addition, myoblast-sheet therapy enhanced cardiac function, corresponding to a 9.2-fold increase in donor cell survival, compared to intramyocardial injection. Both methods achieved reduced infarct size, decreased fibrosis, attenuated cardiomyocyte hypertrophy, and increased neovascular formation, in association with myocardial upregulation of a group of relevant molecules. The pattern of these beneficial changes was similar between two methods, but the degree was more substantial after myoblast-sheet therapy.

Conclusion: The cell-sheet technique enhanced safety and therapeutic efficacy of myoblast-based therapy, compared to the current method, thereby paving the way for clinical application.

1. Introduction

Despite pre-clinical evidence showing that transplantation of skeletal myoblasts (SMBs) greatly improves the function of damaged hearts mainly via the paracrine effect [1], the use of this cell type in clinical cell therapy has been largely curtailed. This was mainly due to two adverse findings in previous clinical studies: occurrence of fatal ventricular arrhythmias and insufficient or inconsistent therapeutic effects [1,2]. We speculate that these issues were associated with the use of a suboptimal cell-delivery method, and that application of a more suitable method may solve both of these concerns.

The commonly used cell-delivery method in previous studies is direct intramyocardial injection of trypsin-treated SMB suspensions [1,2]. This method is, however, known to produce islet-like localized cell-clusters, which could cause disturbance of the electrical conduction, leading to re-entrance arrhythmias [3–5]. In addition, this method is associated with considerable donor cell loss by initial leakage and by cell death/damage due to injection-mediated mechanical injury and subsequent myocardial inflammation. Additional donor cell damage is caused by the enzymatic digestion (i.e. trypsinization) used for cell collection from culture dishes [5–7]. Trypsinization disrupts cell surface proteins and destroys cell–cell connections, thus deteriorating donor cell viability and functionalities. These adverse effects would collectively result in poor donor cell engraftment, which will consequently limit the benefit from this approach [1].

Recent development of the unique culture dish coated with a temperature-responsive polymer (poly-N-isopropylacrylamide) has enabled fabrication of "cell-sheets" simply by reduction of the temperature without any harmful chemical treatment and without using artificial

☆ Grant support: this work was supported by the UK National Institute of Health Research (New and Emerging Applications of Technology Programme (NEAT L018) and Cardiovascular Biomedical Research Unit Award), and the Barts and The London Charity (ETHG1B8R).

* Corresponding author at: William Harvey Research Institute, Barts and The London School of Medicine and Dentistry, Charterhouse Square, London, EC1M 6BQ, UK. Tel.: +44 20 7882 8233; fax: +44 20 7882 8256.
E-mail address: ken.suzuki@qmul.ac.uk (K. Suzuki).

0167-5273/$ – see front matter © 2012 Elsevier Ireland Ltd. All rights reserved.
http://dx.doi.org/10.1016/j.ijcard.2012.09.081

scaffolds [7]. At 37 °C this polymer is hydrophobic, and cells can adhere to the dishes and grow. However, when the temperature is dropped to 25 °C or below, the polymer rapidly becomes hydrophilic, hydrated and swollen, losing its cell-adhesiveness. As a result, the cells detach from the dish as a free cell-sheet. In contrast to trypsinization, cell surface proteins, cell–cell junctions and underpinning extracellular matrix (ECM) are well preserved in this method. Following epicardial placement, cell-sheets are expected to quickly adhere to the heart due to the preserved ECM, minimizing donor cell leakage. Taken together, the epicardial placement of SMB-sheets (SMB-sheet therapy) is likely to achieve greater retention, survival, and engraftment of donor SMBs in the heart while maintaining important donor cell functionalities including the secretion of paracrine mediators, resulting in augmentation of therapeutic benefits, compared to intramyocardial injection. In addition, this innovative method will not produce intramyocardial tissue disruption that disturbs the electrical conductance, and therefore might prevent occurrence of ventricular arrhythmias. In fact, therapeutic effects of SMB-sheet therapy have been reported in various models [8–10]. However, more detailed pre-clinical investigations, particularly on arrhythmia occurrence and other factors concerning the safety and effects, are needed for this approach to be widely established in the clinical arena.

2. Materials and methods

All animal studies were performed with the approval of the institutional ethics committee and the Home Office, UK. The authors of this manuscript have certified that they comply with the Principles of Ethical Publishing in the International Journal of Cardiology. All procedures were carried out in a blind manner whenever possible.

2.1. Generation of SMB-suspensions and SMB-sheets

SMBs were collected from male Lewis rats (150–175 g, Charles River) by the single fiber method as previously described [5,11]. To generate an SMB-sheet, 4×10^6 SMBs (passage 4–5) were seeded on a 35-mm temperature-responsive culture dish (UpCell, CellSeed, Inc.). Following 12–15 h incubation at 37 °C, the temperature was lowered to 22 °C, enabling the SMB-sheet to detach from the dish [8]. For injection, 4×10^6 SMBs were collected using trypsinization and suspended in 200 μl PBS [5]. The size of generated SMB-sheets was approximately 15 mm in diameter. For graft tracking studies, SMBs were labeled with CM-DiI (Molecular Probes) according to the manufacturer's protocol.

2.2. Induction of myocardial infarction (MI) and SMB transplantation

Female Lewis rats (180–200 g, Charles River) underwent left coronary artery ligation as previously described [3,5]. The animals were randomly assigned to receive either SMB-sheet therapy (Sheet group), intramyocardial SMB injection (IM group), or sham-treatment (Cont group). For the Sheet group, an SMB-sheet was epicardially placed to cover the left ventricular (LV) free wall including both infarct and border areas. For the IM group, SMB suspension was injected into 2 sites (100 μl each) of the LV free wall, aiming to target a similar area to SMB-sheet therapy [3,5].

2.3. Measurement of arrhythmia occurrence

Incidence of spontaneous arrhythmias, including premature ventricular contraction (PVC), ventricular tachycardia (VT) and ventricular fibrillation (VF), was continuously monitored by a radio-telemetry system (Data Sciences International) as described previously [3,5]. For accurate evaluation of the arrhythmia severity, the modified Curtis and Walker's scoring system [12] was applied, where frequencies of PVC, VT and VF were systematically taken into account.

2.4. Histological analysis

At chosen time points, the hearts were excised, fixed with 4% paraformaldehyde, and frozen. Cryosections were cut and incubated with polyclonal anti-cardiac troponin-T antibody (1:200 dilution, HyTest), biotin conjugated *Griffonia simplicifolia* lectin I-isolectin B_4 (1:100, Vector), monoclonal anti-CD45 antibody (1:50, BD), monoclonal anti-CD11b antibody (1:50, Chemicon), monoclonal anti-granulocyte antigen (1:20, AbD Serotec), monoclonal OX62 (1:25, AbD Serotec), polyclonal CD3 (1:100, Abcam), or monoclonal connexin43 (Cx43; 1:250, Millipore), followed by visualization using appropriate fluorophore-conjugated secondary antibodies with or without nuclear counter-staining using 4′,6-diamidino-2-phenylindole (DAPI). Ten different fields from each of the border and remote areas per heart were randomly selected and assessed. Another set of sections were stained with 0.1% picrosirius red for assessing infarct size and for detecting collagen deposition [3,5]. To evaluate the cardiomyocyte size, the cross-sectional area of appropriately detected cardiomyocytes [13] was measured of 50 cardiomyocytes in each border and remote area per heart.

2.5. Evaluation of cardiac performance

Cardiac function and dimensions, and hemodynamic parameters were measured by using echocardiography (Vevo-770, VisualSonics) and cardiac catheterization (SPR-320 and PVAN3.2, Millar Instruments) by a blinded operator as previously described [3,5,13].

2.6. Analysis for donor cell survival in the heart and other organs

DNA was extracted from the heart, lung, liver, kidney, and spleen post treatment. The presence of male cells in each female organ was quantitatively assessed to define donor cell presence using real-time PCR (Prism 7900HT, Applied Biosystems) for the Y-chromosome-specific *sry* gene as previously described [3,5]. Non-heart organs that were positively detected for *sry* expression were defined to be ectopic donor cell survival.

2.7. ELISA for myocardial IL-1β levels

Proteins were extracted from the homogenates from frozen whole LV samples collected at day 3 post-treatment with lysis buffer (0.15 M NaCl, 1 mM EDTA, 20 mM Tris pH 7.4, 1 mM DTT and protease inhibitor cocktail (Sigma)). After measuring the protein concentration (BioRad DC protein assay), levels of IL-1β were measured using an ELISA kit (eBioscience) according to the company's instruction.

2.8. Analysis for myocardial gene expression

Total RNA was extracted from frozen whole LV samples and assessed for myocardial gene expression of genes presumably relevant to the SMB-mediated paracrine effect by quantitative RT-PCR (Prism 7900HT) as previously described [14]. TaqMan primers and probes were purchased from Applied Biosystems. Expression was normalized using *Ubiquitin C*.

2.9. Statistical analysis

All values are expressed as mean ± SEM. Statistical comparison of the data was performed using the Student's unpaired *t*-test for the donor cell survival in the heart and using χ^2-test for the ectopic donor cells. Other data were analyzed with one-way ANOVA followed by Fisher's post-hoc analysis to compare groups. A value of $p<0.05$ was considered statistically significant.

3. Results

3.1. Eliminated arrhythmia occurrence by SMB-sheet therapy

We established a rat model to investigate whether the use of the cell-sheet technique might reduce arrhythmogenicity associated with SMB transplantation. Continuous electrocardiogram monitoring using radio-telemetry revealed frequent episodes of premature ventricular contractions (PVCs) in the IM group at both day 1 and 28 (Fig. 1A, C) consistent with previous clinical and experimental reports [1,5], validating the suitability of this model. There was a smaller number of PVC occurrence observed in the Cont group, which is also commonly seen post-MI [5,11], and more importantly the frequency of PVCs in the Sheet groups was just comparable to this base-line data. Furthermore, the IM group showed more frequent ventricular tachycardia (VT) occurrence than other groups; more than one-third of the animals in the IM group developed VT (Fig. 1B, D). Furthermore, one animal of the IM group developed transient ventricular fibrillation (VF) at day 28. In contrast, there was no animal that developed VT or VF in the Sheet group throughout the period studied. Consequently, the IM group, but not Sheet group, showed a higher arrhythmia score than the Cont group (Fig. 1E). These data are the first quantitative evidence that SMB transplantation-induced arrhythmogenicity can be prevented by the use of the cell-sheet technique.

3.2. Donor cell behaviors after SMB-sheet therapy

To gain an insight of the mechanism by which SMB-sheet therapy attenuated arrhythmogenicity, we first assessed the quantitative donor cell survival (presence). As a result, the donor cell presence in the heart in the Sheet group was 3.5-fold and 9.2-fold higher than that in the IM

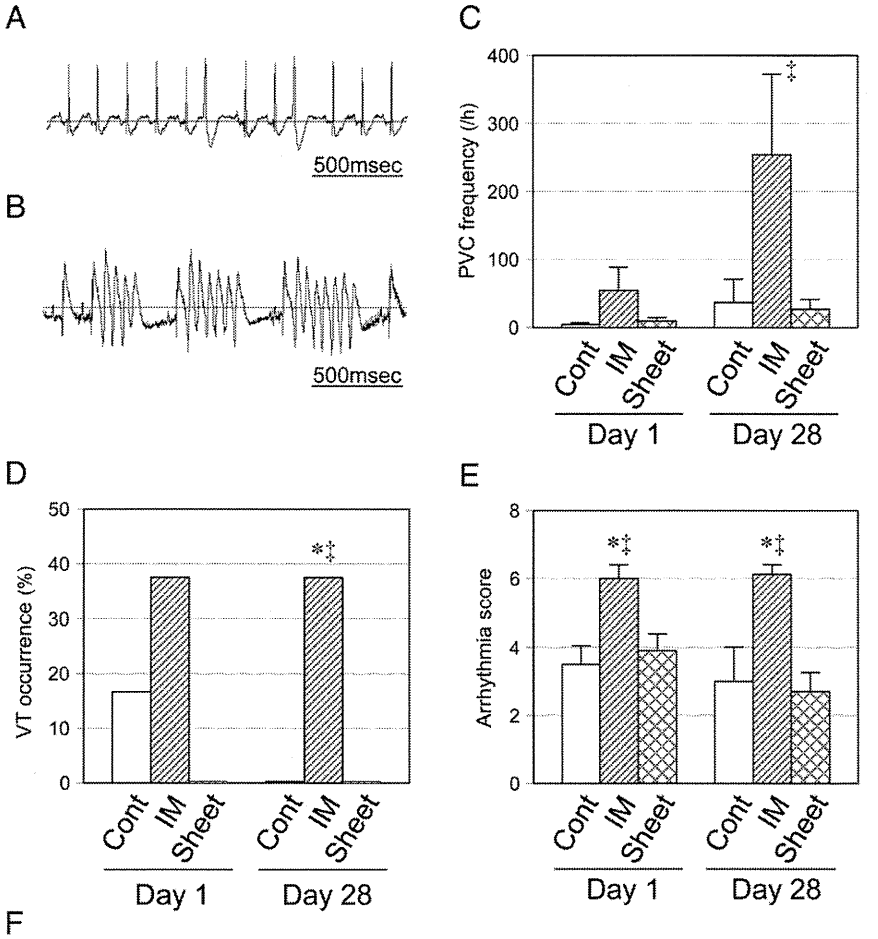

F

	RR (msec)	P (msec)	PR (msec)	QRS (msec)	QTc (msec)
Cont	148.3±9.6	18.3±1.3	42.1±0.8	18.1±0.4	5.8±0.4
IM	159.2±11.0	20.7±2.0	43.5±1.3	20.1±0.7*‡	5.9±0.1
Sheet	155.8±7.5	19.6±0.7	43.1±1.3	17.1±0.4	5.4±0.1

Fig. 1. Eliminated arrhythmogenicity by SMB-sheet therapy. Arrhythmia occurrence was assessed by continuous electrocardiogram monitoring using radio-telemetry. Representative patterns of PVC (A) and VT (B) in the IM group at day 28 are shown. The IM group, but not the Sheet group, increased the occurrence of PVC (C) and VT (D; % animals) and consequently elevated the arrhythmia score (E; accumulated hourly scores for 6 h), in association with elongated QRS duration, at day 28 (F), compared to the Cont group. *$p<0.05$ vs. Cont group, ‡$p<0.05$ vs. Sheet group, $n=6$–8 in the Cont, IM, and Sheet groups, respectively.

group at day 3 and 28, respectively (Fig. 2A). This meant that SMB-sheet therapy achieved much greater SMB existence in the heart, but contradictorily reduced arrhythmia occurrence, suggesting that changes in the donor size was not a reason for the eliminated arrhythmogenicity after SMB-sheet therapy. We then looked into the differences in distribution and associated behaviors of SMBs between two methods by histological studies with tracking CM-DiI-labeled SMBs. As expected from previous studies [5], the IM group formed islet-like, localized cell-clusters composed of donor SMBs and host $CD45^+$ inflammatory cells at day 3 (Fig. 2B, F), which persisted up to day 28 with a reduced size (Fig. 2C, G). In addition, immunolabelling for Cx43 demonstrated that grafted SMBs expressed Cx43 protein (though to a limited extent) within the cell-clusters at day 3 in the IM group (Fig. 2J), but there was no Cx43-containing gap junction formation between SMBs and cardiomyocytes on day 3 or 28 (Fig. 2J, K). In contrast, the donor cell distribution was markedly different after SMB-sheet therapy; the majority of donor cells remained on the epicardial surface at both day 3 and 28 in the Sheet group, thus obviating the induction of myocardial heterogeneity or disruption (Fig. 2D, E, H, I). Also, there was no gap junction formation between SMB-sheets and cardiomyocytes after SMB-sheet therapy (Fig. 2L, M). Collectively, intramyocardial SMB injection caused the donor cell clusters with intense inflammation within the myocardium, which was electrically isolated from host cardiomyocytes, causing physical disturbance to electrical impulse propagation, and resulting in conduction delay, block, and eventually re-entrance arrhythmias. In contrast, SMBs were localized on the epicardial surface (outside myocardium) after cell-sheet placement and did not affect the electrical conductance of the host heart. Corresponding to these findings, the QRS duration was elongated at day 28 in the IM group compared to other groups (Fig. 1F).

3.3. Prevention of exacerbation of myocardial inflammation by SMB-sheet therapy

Another possible mechanism by which SMB transplantation induces ventricular arrhythmias may be an increase in the arrhythmogenic substrates, including inflammatory response. Post-MI failing cardiomyocytes

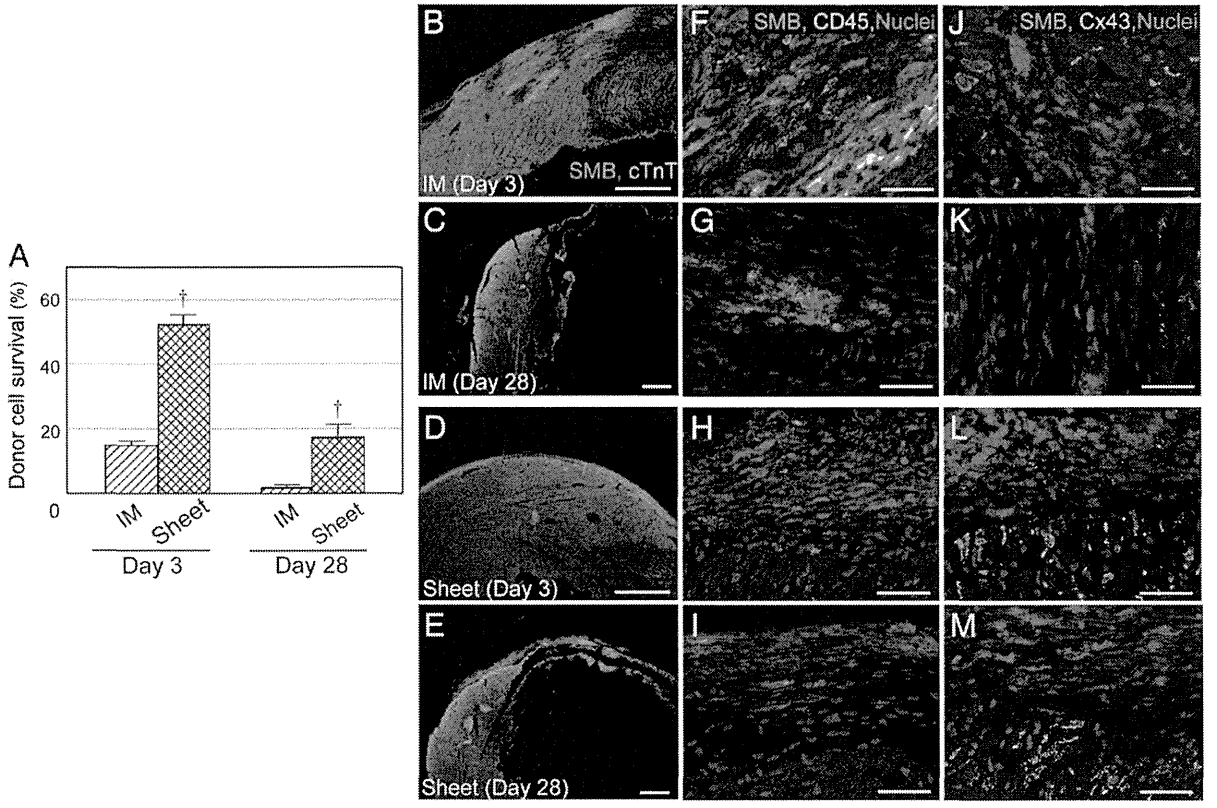

Fig. 2. Donor cell behaviors after SMB-sheet therapy. Quantitative assessments showed that donor cell survival (% of donor cell number existing in the heart) was higher in the Sheet group than in the IM group at both day 3 and 28 (A). †$p<0.01$ vs. IM group, $n=4$–6 in each point. Immunofluorescence showed that clusters of SMBs and $CD45^+$ inflammatory cells were formed in the IM group at day 3 (B, F) and 28 (C, G), while these intramyocardial heterogeneities were absent in the Sheet group, in which most of donor cells retained on the epicardial surface (D, H for day 3; E, I for day 28). Immunolabelling for Cx43 showed that there was no obvious gap junction formation between SMBs and host cardiomyocytes in both the IM (J, K) or Sheet group (L, M) at either day 3 or 28. Orange signals for SMBs (CM-DiI); blue for nuclei (DAPI); green for cardiac Troponin-T (cTnT) in (B–E), for CD45 in (F–I) or for Cx43 (J–M). Scale bar = 1 mm in (B–E) and 30 μm in (F–M).

suffer adverse alterations of cellular properties including inappropriate gap junction expression/distribution and electrical instability, which will increase vulnerability to arrhythmogenic stimuli [15]. Our immunolabeling analyses demonstrated that there was increased accumulation of $CD45^+$ inflammatory cells globally into the host myocardium post MI, both at border and remote areas, in the Cont group (Fig. 3A). More importantly, this inflammatory response was further exacerbated in the IM group widely and persistently, while in contrast this exacerbation was prevented in the Sheet group. The IM group increased the accumulation of granulocytes (Fig. 3B), $CD11b^+$ monocytes/macrophages (Fig. 3C), and $OX62^+$ dendritic cells (Fig. 3D) into the border areas at both day 3 and 28, compared to other groups. Correspondingly, the myocardial level of a major pro-inflammatory cytokine, IL-1β, was significantly increased in the IM group, compared to the Cont group, whereas this increase was entirely absent after SMB-sheet therapy (Fig. 3E). IL-1β is known to increase arrhythmia susceptibility by increasing the Ca_2^+ leak from the sarcoplasmic reticulum [16]. These data collectively showed that intramyocardial SMB injection exacerbated inflammation and increased susceptibility of arrhythmias, while this adverse effect was obviated by SMB-sheet therapy.

3.4. Attenuated donor cell leakage into the lung by SMB-sheet therapy

During this study, we unexpectedly found another safety concern associated with intramyocardial SMB injection. PCR for the *sry* gene in various organ samples detected a substantial presence of male donor cells in the lungs of all host female animals at day 28 in the IM group (Fig. 4A). Consistent with this, donor cell trafficking studies using CM-DiI-labeled SMBs uncovered that there were a considerable number of donor cells globally distributing in the lung, forming discrete loci (Fig. 4C, D). It has been reported that many donor cells leak into other organs, commonly the lung and kidney, at early phases of intramyocardial injection of bone marrow-derived cells [17]. This aspect in the case of SMBs remains largely unexplored, and our study clarified that after intramyocardial SMB injection a considerable number of donor cells leaked and survived in the lung for at least 28 days. In contrast, in the Sheet group, no donor cells were detected in any organ studied, by either PCR or histological study (Fig. 4A, B), shedding the light on a further advantage of SMB-sheet therapy in safety over the current method, in addition to the elimination of arrhythmogenicity.

3.5. Improved cardiac performance by SMB-sheet therapy

Previous clinical trials of intramyocardial injection of SMB suspension showed insufficient or inconsistent therapeutic effects, in corresponding with poor donor cell survival/engraftment [1,2]. Considering the ability to increase donor cell survival (Fig. 2A), the use of the cell-sheet technique may solve this issue. Indeed, echocardiography showed that LV ejection fraction was improved in the IM group compared to the Cont group, and this was further enhanced in the Sheet group at day 28 post treatment (Fig. 5A). In addition, both LV end-diastolic and end-systolic dimensions in the Sheet group were smaller than those in other groups (Fig. 5B, C). Cardiac catheterization also showed improved cardiac function in the Sheet group compared to the other groups (Fig. 5E). LV end-diastolic

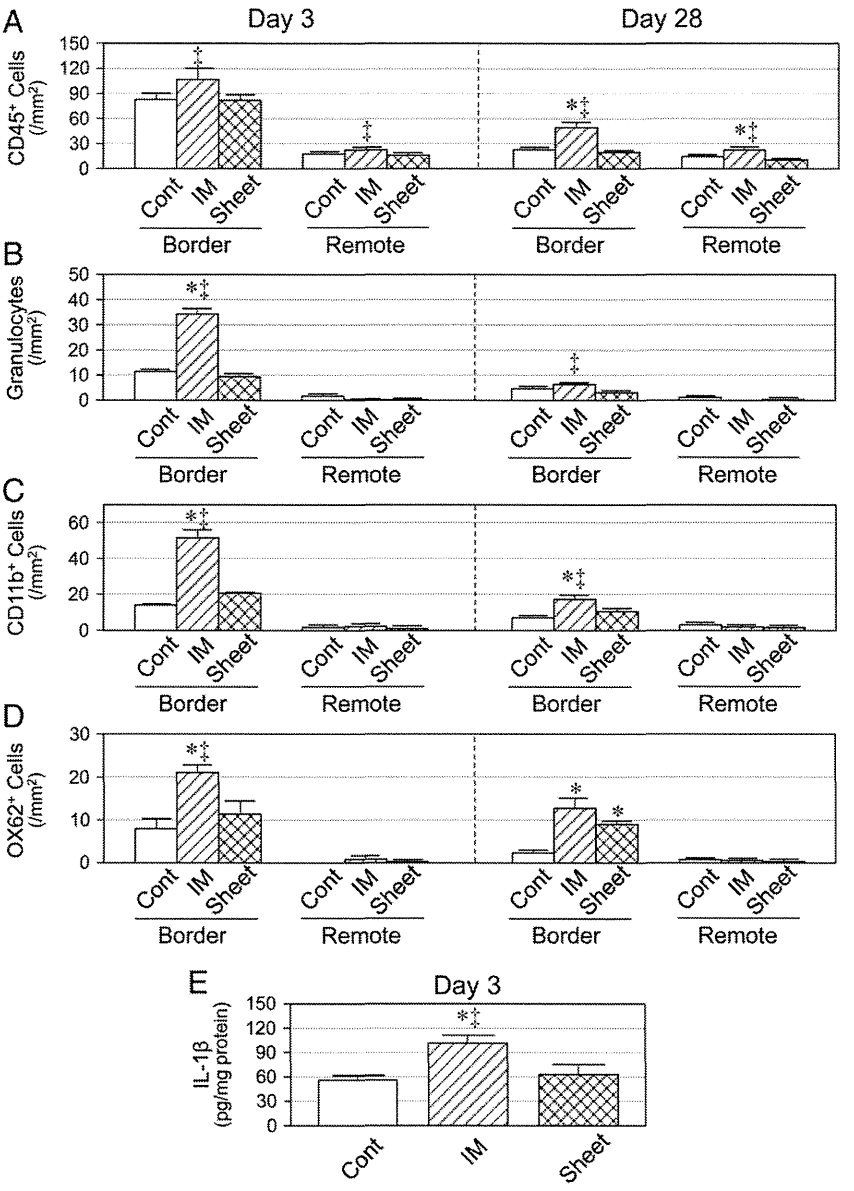

Fig. 3. Prevention of exacerbation of myocardial inflammation by SMB-sheet therapy. Immunolabeling demonstrated that the number of $CD45^+$ cells accumulating in the myocardium was persistently increased in the IM group, but not in the Sheet group, widely in both border and remote areas (A). In addition, in the IM group, there was increased accumulation of granulocytes (B), $CD11b^+$ monocytes/macrophages (C), and $OX62^+$ dendritic cells (D) at both day 3 and 28. ELISA showed increased myocardial IL-1β levels at day 3 in the IM group compared to other groups (E). $^*p<0.05$ vs. Cont group, $^‡p<0.05$ vs. Sheet group, n = 4–6 in each group.

pressure was lower and developed pressure was higher in the Sheet group compared to the Cont group.

3.6. Mechanisms underpinning the therapeutic effects of SMB-sheet therapy

We subsequently studied the mechanism by which SMB-sheet therapy improved cardiac function. Agreeing with previous findings [1,5], we could not find any cardiomyocyte-like cells derived from donor SMBs (via either trans-differentiation or fusion) in any group by histological trafficking of CM-DiI labeled SMBs. Instead, our histological studies detected favorable changes in each cardiac component in the Sheet group. These included reduced infarct size (Fig. 5D), decreased extracellular collagen deposition (Fig. 6A–G), increased vascular formation (Fig. 6H–N), and attenuated cardiomyocyte hypertrophy (Fig. 6O–R) at day 28 in the Sheet group compared o the Cont group. Of note, these beneficial effects were widely observed not only in the border areas but also in the remote areas. These beneficial changes were also seen in the IM group, but to a reduced extent in general, correlated with the reduced donor SMB presence.

To obtain a further mechanistic insight of the therapeutic effects of SMB-sheet therapy, we analyzed myocardial expression of reportedly relevant genes by quantitative RT-PCR. As a result, we observed that expression of *IL-10*, *HIF1-α*, *MMP-2*, *TIMP-1*, *IGF-1*, and *SDF-1*, was significantly upregulated in the Sheet group at day 3 compared to the Cont group (Fig. 7). These data corresponded well with the above histological findings of beneficial changes in cardiac components as the paracrine effects. An anti-inflammatory cytokine, *IL-10*, is known to increase donor cell survival after cell transplantation and also increase angiogenesis [18]. Upregulation of a major pro-angiogenic factor, *HIF1-α* [19], could also play a role in the increased capillary density in the Sheet group, while upregulation in *MMP-2* and *TIMP-1* would correlate with the reduced fibrosis [3]. Upregulation of *IGF-1* and *SDF-1*, which are known to stimulate endogenous progenitor cells [20,21], might have increased endogenous regeneration. Of note, the upregulation of these genes in the Sheet group was mostly reduced to the post-MI background level

A

	Lung	Liver	Spleen	Kidney
IM	4/4 (100%)	0/4 (0%)	1/4 (25%)	1/4 (25%)
Sheet	0/4 (0%)	0/4 (0%)	0/4 (0%)	0/4 (0%)
p value	0.0047	NS	NS	NS

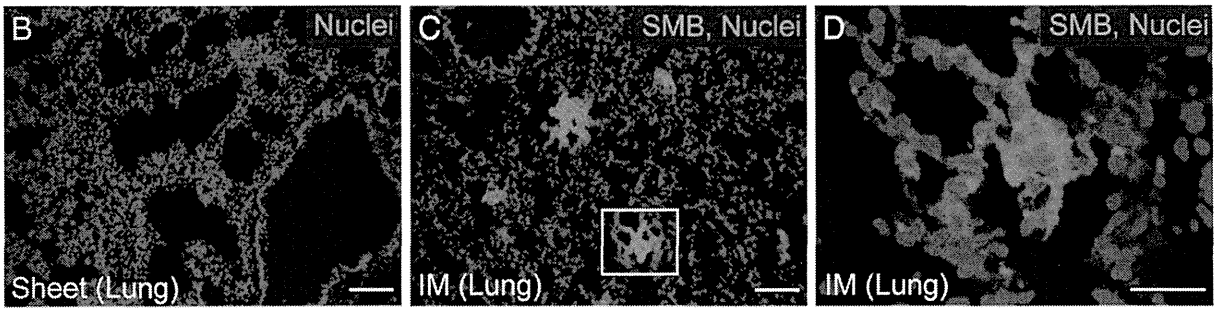

Fig. 4. Attenuated ectopic donor cells in other organs after SMB-sheet therapy. At day 28 post treatment, PCR for *sry* detected the presence of donor cells in the lungs of all host animals in the IM groups (A). There were no donor cells detected in any organs after SMB-sheet therapy. Fluorescence observation demonstrated that SMBs (CM-DiI-labeled; orange) were widely distributed in the lung, forming discrete loci, at day 28 in the IM group (C, D), while there were no SMBs detected in the lung of the Sheet group (B). Blue (DAPI) represents nuclei. Scale bar = 100 μm in (B, C) and 30 μm in (D).

in the Cont group by day 28, in corresponding with the reduced donor cell presence by day 28 (Fig. 2A). Despite this, cardiac function remained improved for at least 28 days after SMB-sheet therapy compared to the sham control. This let us speculate that paracrine mediators would contribute to the myocardial recovery mainly during the early phase after the treatment, and the effects on cardiac function and structure, once established, could last for a longer time.

4. Discussion

This pre-clinical study demonstrated that epicardial placement of SMB-sheets, which were generated with temperature-responsive culture dishes without enzymatic treatment and without artificial scaffolds, overcame both key problems of the current SMB transplantation method: critical arrhythmogenicity and limited therapeutic efficacy [1,2].

This study for the first time provided comprehensive, quantitative evidence showing that the use of the cell-sheet technique prevents arrhythmogenicity associated with SMB-transplantation therapy to the heart. We established a rat model in which intramyocardial SMB injection induced frequent ventricular arrhythmias, including VT, in an equivalent manner to the previous clinical reports [1,2,22]. Using this clinically-relevant model, our continuous monitoring using radio-telemetry clearly demonstrated that arrhythmia occurrence was reduced after SMB-sheet therapy to the base line (MI hearts; Cont group). Together with another novel finding that SMB-sheet therapy attenuated ectopic donor cell distribution in the lung, which was seen after intramyocardial injection, these data highlight the improved safety of SMB-sheet therapy.

Furthermore, our results also imply information regarding the mechanism underlying SMB-induced arrhythmias, which remains uncertain [22]. Previous *in vitro* studies have suggested a possible role of automaticity or spontaneous electrical activity of the SMBs on the

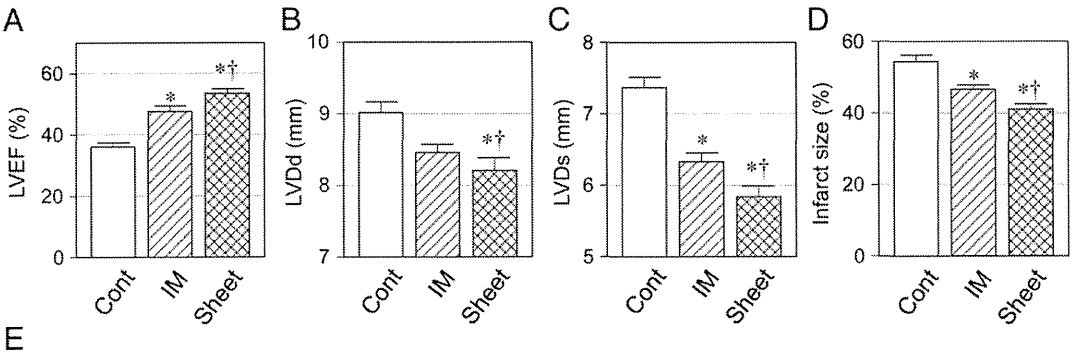

E

	HR (bpm)	LVEDP (mmHg)	LVDP (mmHg)	Max dP/dt (mmHg/s)	Min dP/dt (mmHg/s)	Contractility Index
Cont	375±8	18.1±1.2	79.7±1.8	6832±138	-5686±351	105.9±3.6
IM	376±9	12.8±0.9*	95.7±3.1*	7598±277*	-6764±413	119.0±4.1*
Sheet	368±7	10.8±1.2*	105.4±4.3*†	8707±311*†	-7558±350*	124.1±5.3*

Fig. 5. Improved cardiac performance by SMB-sheet therapy. Enhanced cardiac function, reduced heart dimensions and improved hemodynamics in the Sheet group, compared to other groups, were detected by using echocardiography (A–C) and catheterization (E) at day 28. Picrosirius red staining showed the smallest infarct size in the Sheet group (D). HR = heart rate, LVDd = LV end-diastolic dimension, LVDs = LV end-systolic dimension, LVEDP = LV end-diastolic pressure, LVDP = LV developed pressure, *$p<0.05$ vs. Cont group, †$p<0.05$ vs. IM group, n = 10–11 in each group in (A–C), 4–5 in (D), and 7–8 in (E).

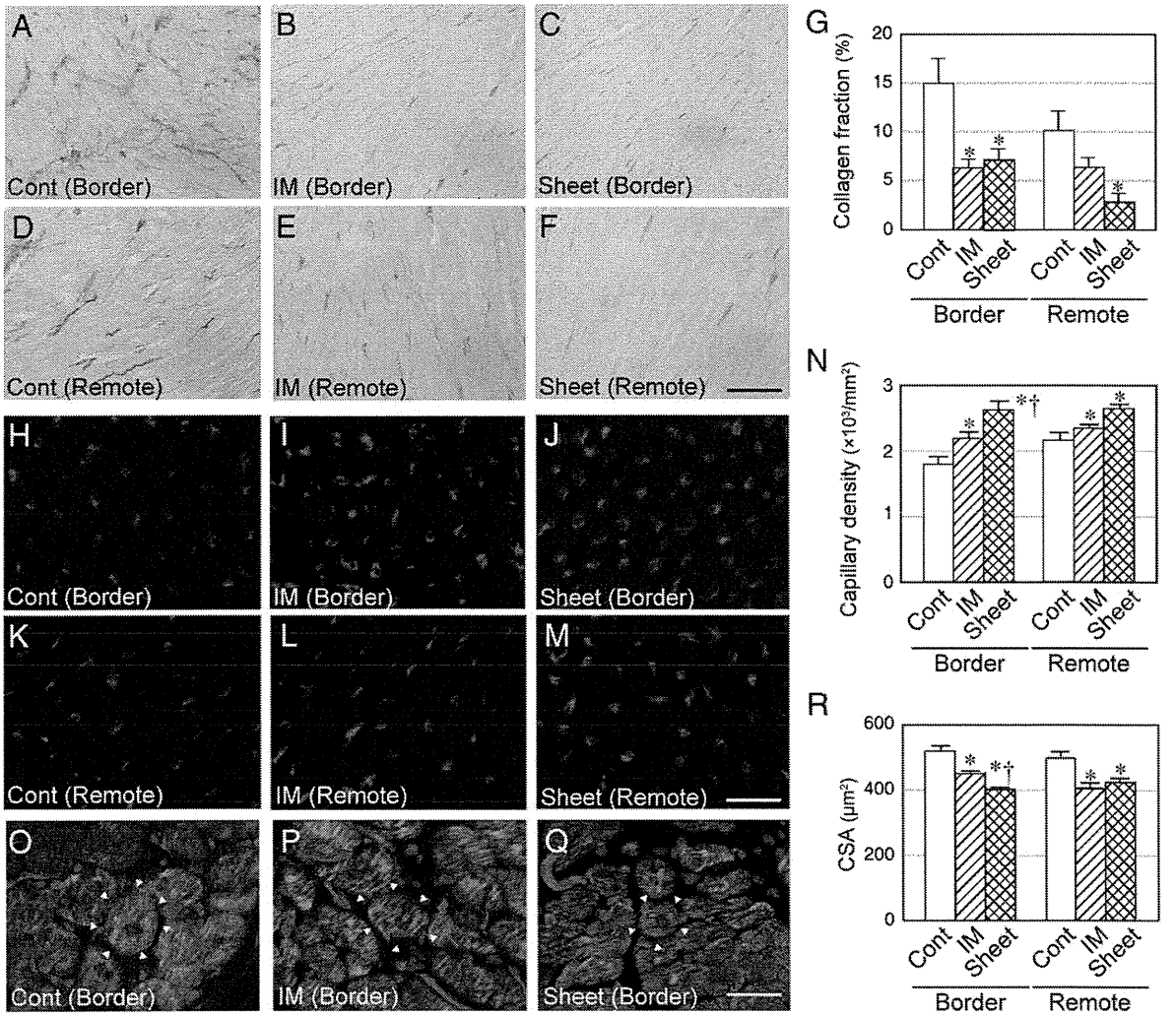

Fig. 6. Recovery of post-MI failing myocardium by SMB-sheet therapy. Picrosirius red staining showed that extracellular collagen deposition (red color) in the Cont group (A, D) was reduced in the IM (B, E) and Sheet groups (C, F) at day 28. Semi-quantified collagen volume fraction is shown in (G). Isolectin B_4 staining demonstrated that capillary density (red color) at day 28 was increased in the IM (I, L) and Sheet groups (J, M) compared to the Cont group (H, K). Capillary density was quantified as the number of capillary vessels per mm^2 (N). Cardiomyocyte size (CSA = cross sectional area) was reduced in the Sheet group compared to the Cont group (O–R). Green signals for cardiomyocytes (cTnT); red for endothelial cells (Isolectin B4). Cells surrounded by white arrowheads represent the cardiomyocytes chosen for the CSA measurement. Scale bar = 100 μm in (A–F) and 30 μm in (H–M, O–Q). $^{*}p<0.05$ vs. Cont group, $^{\dagger}p<0.05$ vs. IM group, n = 4–6 in each group.

arrhythmogenicity [23,24]; however, results of our *in vivo* study were rather negative for these, as the cell-sheet technique showed reduced arrhythmogenicity despite the increase in surviving SMBs. Alternatively, our results propose that the formation of local heterogeneity by intramyocardial injection may play a causative role [4,5,22]. We observed that intramyocardial injection formed discrete cell-clusters composed of donor SMBs and host inflammatory cells. Given our histological finding that grafted SMBs rarely formed gap junctions with host cardiomyocytes, such intramyocardial heterogeneity would cause physical disturbance to electrical impulse propagation, resulting in conduction delay, block, and eventually re-entrance arrhythmias. This concept was supported by additional finding of the elongated QRS duration after intramyocardial SMB injection. In contrast, after SMB-sheet therapy, the majority of SMBs remained on the epicardial surface, obviating the intramyocardial tissue disruption. This resulted in the maintenance of electrical conductance, therefore preventing arrhythmogenicity. In addition, this study provided new data which suggest another mechanism by which intramyocardial SMB injection induced arrhythmias; exacerbation of post-MI arrhythmogenic substrates [12,22]. Intramyocardial SMB injection resulted in persistent and widespread increase of inflammatory response, which could amplify the pathological substrates and increase arrhythmia susceptibility. In contrast, SMB-sheet therapy did not aggravate myocardial inflammation nor therefore increase arrhythmogenic substrates.

Insufficient therapeutic efficacy was another key issue of SMB transplantation [1,2], and this may also be solved by the use of the cell-sheet technique. It has been shown that SMB-sheet therapy improves performance of the damaged heart in various models [8–10], but this study further confirms this ability of SMB-sheet therapy in a more comprehensive manner by direct comparison with intramyocardial injection. In addition, we showed that this augmented efficacy was correlated to the increased donor cell engraftment. Our quantitative assessment showed that donor cell survival at day 3 was 3.5-fold higher in SMB-sheet therapy compared to intramyocardial injection, suggesting that the use of the cell-sheet technique increased the early retention and/or survival of donor cells. Furthermore, the surviving donor cell number at day 28 was more apparent, 9.2-fold, larger in SMB-sheet therapy. This indicates that SMBs grafted by the cell-sheet technique survived between day 3 and 28 with a higher rate (17.5/52.3 = 0.33) compared to intramyocardial injection (1.9/15.0 = 0.13), suggesting that the cell-sheets would provide a more comfortable environment for SMBs to survive.

Consistent to previous reports [1,5], we did not find donor SMB-derived cardiomyocytes either after SMB-sheet therapy or intramyocardial SMB

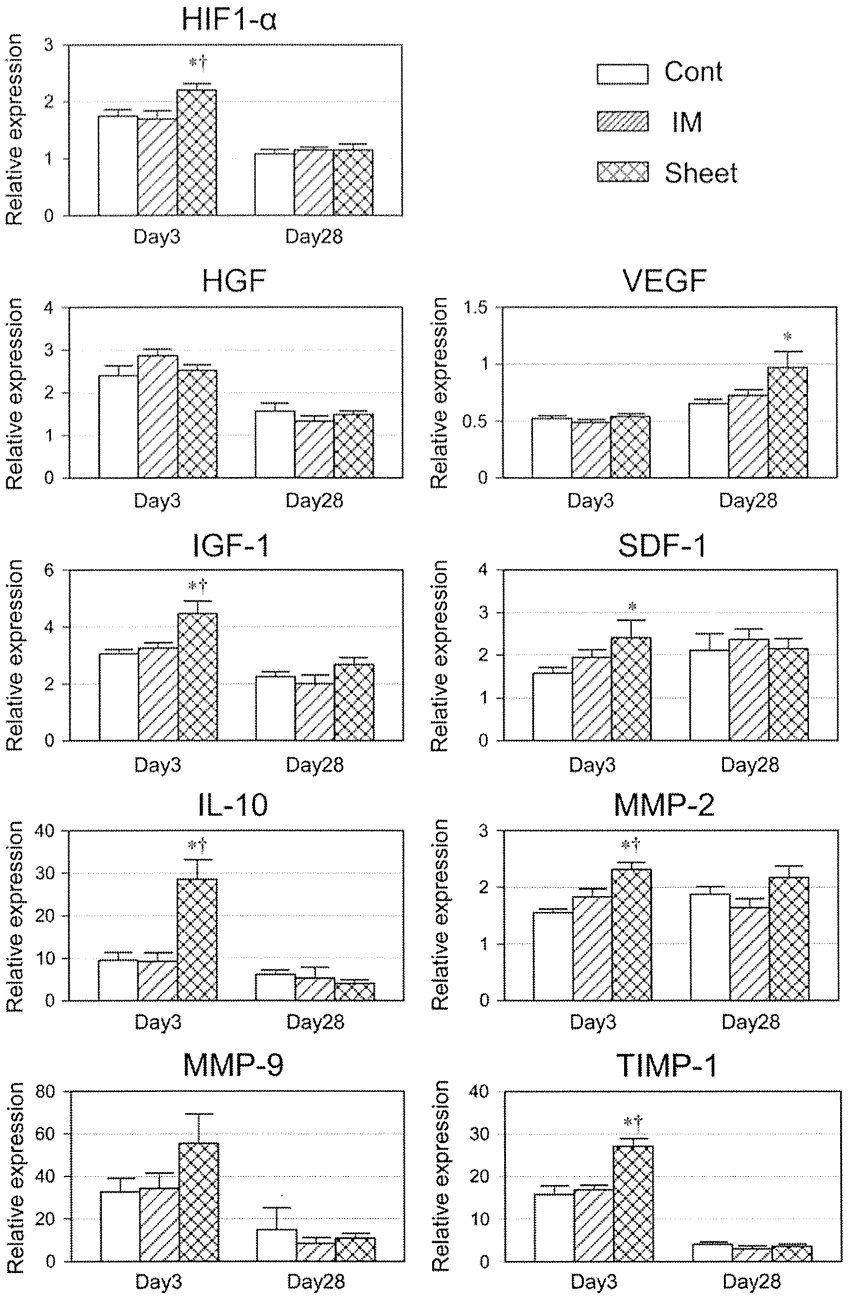

Fig. 7. Myocardial gene expression after SMB-sheet therapy. Quantitative RT-PCR detected upregulation of multiple genes in the Sheet group at day 3, though this was largely diminished by day 28. Expression levels were normalized to that in normal hearts (n = 3), which was assigned a value of 1.0. *p<0.05 vs. Cont group, †p<0.05 vs. IM group, n = 4–6 in each group.

injection. Considering the beneficial histological changes, including decreased infarct size, reduced fibrosis, increased neovascular formation, and attenuation of cardiomyocyte hypertrophy, the "paracrine effect" may be the major mechanism responsible for the therapeutic benefits by SMB-sheet therapy. As regards this, we found that a group of possibly relevant molecules, including *IL-10*, *HIF1-α*, *MMP-2*, *TIMP-1*, *IGF-1* and *SDF-1*, were upregulated in the heart after SMB-sheet therapy. We could not specify what paracrine molecules among these (or others) were really responsible for the effects of SMB-sheet therapy, but speculate that the obtained effects may be a result of the net input of certain groups of paracrine molecules, rather than a single molecule. However, further investigation is needed to conclude this issue.

In conclusion, SMB-sheet therapy attenuated both the arrhythmogenicity and ectopic donor cell distribution in the lung that were associated with the current method for SMB transplantation, together with augmented therapeutic efficacy in the treatment of heart failure. These data may encourage the development of this emerging approach towards clinical application.

References

[1] Menasche P. Cell-based therapy for heart disease: a clinically oriented perspective. Mol Ther 2009;17:758-66.
[2] Menasche P, Alfieri O, Janssens S, et al. The Myoblast Autologous Grafting in Ischemic Cardiomyopathy (MAGIC) trial: first randomized placebo-controlled study of myoblast transplantation. Circulation 2008;117:1189-200.
[3] Fukushima S, Varela-Carver A, Coppen SR, et al. Direct intramyocardial but not intracoronary injection of bone marrow cells induces ventricular arrhythmias in a rat chronic ischemic heart failure model. Circulation 2007;115:2254-61.
[4] Gepstein L, Ding C, Rehemedula D, et al. *In vivo* assessment of the electrophysiological integration and arrhythmogenic risk of myocardial cell transplantation strategies. Stem Cells 2010;28:2151-61.
[5] Fukushima S, Coppen SR, Lee J, et al. Choice of cell-delivery route for skeletal myoblast transplantation for treating post-infarction chronic heart failure in rat. PLoS One 2008;3:e3071.

[6] Suzuki K, Murtuza B, Beauchamp JR, et al. Dynamics and mediators of acute graft attrition after myoblast transplantation to the heart. FASEB J 2004;18:1153-5.
[7] Nagase K, Kobayashi J, Okano T. Temperature-responsive intelligent interfaces for biomolecular separation and cell sheet engineering. J R Soc Interface 2009;6(Suppl. 3):S293-309.
[8] Memon IA, Sawa Y, Fukushima N, et al. Repair of impaired myocardium by means of implantation of engineered autologous myoblast sheets. J Thorac Cardiovasc Surg 2005;130:1333-41.
[9] Miyagawa S, Saito A, Sakaguchi T, et al. Impaired myocardium regeneration with skeletal cell sheets—a preclinical trial for tissue-engineered regeneration therapy. Transplantation 2010;90:364-72.
[10] Kondoh H, Sawa Y, Miyagawa S, et al. Longer preservation of cardiac performance by sheet-shaped myoblast implantation in dilated cardiomyopathic hamsters. Cardiovasc Res 2006;69:466-75.
[11] Opitz CF, Mitchell GF, Pfeffer MA, Pfeffer JM. Arrhythmias and death after coronary artery occlusion in the rat. Continuous telemetric ECG monitoring in conscious, untethered rats. Circulation 1995;92:253-61.
[12] Curtis MJ, Walker MJ. Quantification of arrhythmias using scoring systems: an examination of seven scores in an *in vivo* model of regional myocardial ischaemia. Cardiovasc Res 1988;22:656-65.
[13] Litwin SE, Raya TE, Anderson PG, Litwin CM, Bressler R, Goldman S. Induction of myocardial hypertrophy after coronary ligation in rats decreases ventricular dilatation and improves systolic function. Circulation 1991;84:1819-27.
[14] Shintani Y, Fukushima S, Varela-Carver A, et al. Donor cell-type specific paracrine effects of cell transplantation for post-infarction heart failure. J Mol Cell Cardiol 2009;47:288-95.
[15] Severs NJ, Bruce AF, Dupont E, Rothery S. Remodelling of gap junctions and connexin expression in diseased myocardium. Cardiovasc Res 2008;80:9–19.
[16] Duncan DJ, Yang Z, Hopkins PM, Steele DS, Harrison SM. TNF-alpha and IL-1beta increase Ca_2^{+} leak from the sarcoplasmic reticulum and susceptibility to arrhythmia in rat ventricular myocytes. Cell Calcium 2010;47:378-86.
[17] Li SH, Lai TY, Sun Z, et al. Tracking cardiac engraftment and distribution of implanted bone marrow cells: comparing intra-aortic, intravenous, and intramyocardial delivery. J Thorac Cardiovasc Surg 2009;137:1225-33.
[18] Burchfield JS, Iwasaki M, Koyanagi M, et al. Interleukin-10 from transplanted bone marrow mononuclear cells contributes to cardiac protection after myocardial infarction. Circ Res 2008;103:203-11.
[19] Huang Y, Hickey RP, Yeh JL, et al. Cardiac myocyte-specific HIF-1alpha deletion alters vascularization, energy availability, calcium flux, and contractility in the normoxic heart. FASEB J 2004;18:1138-40.
[20] Askari AT, Unzek S, Popovic ZB, et al. Effect of stromal-cell-derived factor 1 on stem-cell homing and tissue regeneration in ischaemic cardiomyopathy. Lancet 2003;362: 697-703.
[21] Santini MP, Tsao L, Monassier L, et al. Enhancing repair of the mammalian heart. Circ Res 2007;100:1732-40.
[22] Menasche P. Stem cell therapy for heart failure: are arrhythmias a real safety concern? Circulation 2009;119:2735-40.
[23] Itabashi Y, Miyoshi S, Yuasa S, et al. Analysis of the electrophysiological properties and arrhythmias in directly contacted skeletal and cardiac muscle cell sheets. Cardiovasc Res 2005;67:561-70.
[24] Abraham MR, Henrikson CA, Tung L, et al. Antiarrhythmic engineering of skeletal myoblasts for cardiac transplantation. Circ Res 2005;97:159-67.

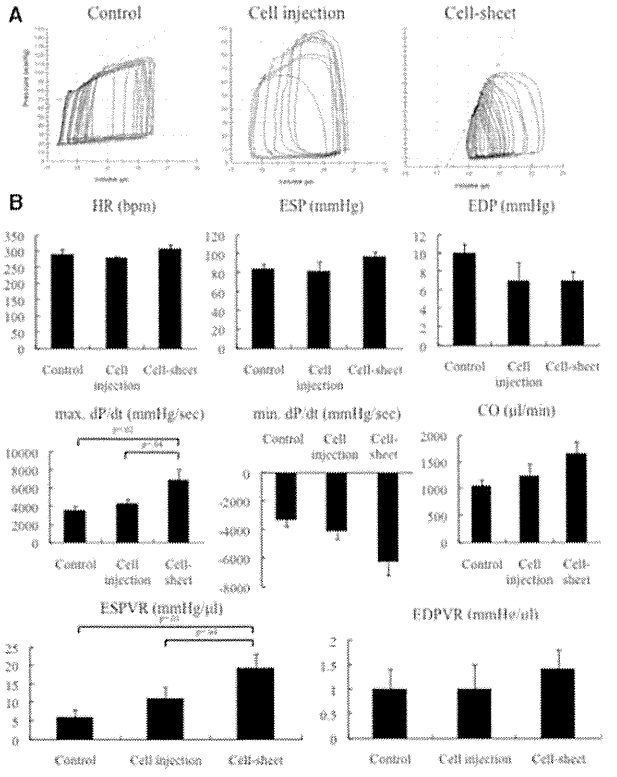

Figure 7.

Hemodynamic measurements determined using cardiac catheterization after cocultured bi-level cell-sheet transplantation (cell-sheet, n=6), cocultured cell injection (cell injection, n=6), and control (control, n=8). Examinations were performed at 4 weeks of follow-up after the operation. **A**, Representative pressure–volume loops during inferior vena cava occlusion from cell-sheet, cell injection, and control groups. **B**, There was no significant difference in heart rate (HR), end-systolic pressure (ESP), end-diastolic pressure (EDP), mimimal rate of change in left ventricular (LV) pressure (min. d*P*/d*t*), cardiac output (CO), or end-diastolic pressure–volume relationship (EDPVR; HR, *P*=0.35; ESP, *P*=0.19; EDP, *P*=0.14; min. d*P*/d*t*, *P*=0.05; CO, *P*=0.07; EDPVR, *P*=0.70; Kruskal–Wallis test). The maximal rate of change in LV pressure (max. d*P*/d*t*) and end-systolic pressure–volume relationship (ESPVR) significantly improved in the cell-sheet group compared with the other 2 groups (max. d*P*/d*t*, *P*=0.04; ESPVR, *P*=0.03; Kruskal–Wallis test).

PLOS ONE

Sustained-Release Delivery of Prostacyclin Analogue Enhances Bone Marrow-Cell Recruitment and Yields Functional Benefits for Acute Myocardial Infarction in Mice

Yukiko Imanishi[1], Shigeru Miyagawa[1], Satsuki Fukushima[1], Kazuhiko Ishimaru[1], Nagako Sougawa[1], Atsuhiro Saito[2], Yoshiki Sakai[3], Yoshiki Sawa[1]*

1 Department of Cardiovascular Surgery, Graduate School of Medicine, Osaka University, Osaka, Japan, **2** Medical Center for Translational Research, Osaka University Hospital, Osaka, Japan, **3** Research Headquarters, ONO Pharmaceutical CO., LTD., Osaka, Japan

Abstract

Background: A prostacyclin analogue, ONO-1301, is reported to upregulate beneficial proteins, including stromal cell derived factor-1 (SDF-1). We hypothesized that the sustained-release delivery of ONO-1301 would enhance SDF-1 expression in the acute myocardial infarction (MI) heart and induce bone marrow cells (BMCs) to home to the myocardium, leading to improved cardiac function in mice.

Methods and Results: ONO-1301 significantly upregulated SDF-1 secretion by fibroblasts. BMC migration was greater to ONO-1301-stimulated than unstimulated conditioned medium. This increase was diminished by treating the BMCs with a CXCR4-neutralizing antibody or CXCR4 antagonist (AMD3100). Atelocollagen sheets containing a sustained-release form of ONO-1301 (n = 33) or ONO-1301-free vehicle (n = 48) were implanted on the left ventricular (LV) anterior wall immediately after permanent left-anterior descending artery occlusion in C57BL6/N mice (male, 8-weeks-old). The SDF-1 expression in the infarct border zone was significantly elevated for 1 month in the ONO-1301-treated group. BMC accumulation in the infarcted hearts, detected by in vivo imaging after intravenous injection of labeled BMCs, was enhanced in the ONO-1301-treated hearts. This increase was inhibited by AMD3100. The accumulated BMCs differentiated into capillary structures. The survival rates and cardiac function were significantly improved in the ONO-1301-treated group (fractional area change 23±1%; n = 22) compared to the vehicle group (19±1%; n = 20; P = 0.004). LV anterior wall thinning, expansion of infarction, and fibrosis were lower in the ONO-1301-treated group.

Conclusions: Sustained-release delivery of ONO-1301 promoted BMC recruitment to the acute MI heart via SDF-1/CXCR4 signaling and restored cardiac performance, suggesting a novel mechanism for ONO-1301-mediated acute-MI heart repair.

Citation: Imanishi Y, Miyagawa S, Fukushima S, Ishimaru K, Sougawa N, et al. (2013) Sustained-Release Delivery of Prostacyclin Analogue Enhances Bone Marrow-Cell Recruitment and Yields Functional Benefits for Acute Myocardial Infarction in Mice. PLoS ONE 8(7): e69302. doi:10.1371/journal.pone.0069302

Editor: Toru Hosoda, Tokai University, Japan

Received February 8, 2013; **Accepted** June 6, 2013; **Published** July 19, 2013

Funding: This study was funded by grant-in-aid for Core-to-Core Program (21003) from the Japan Society for the Promotion of Science (http://jsps-osaka-u.jpn.org/en/index.html), early-stage and exploratory clinical trial centers project from the Ministry of Health (http://jsps-osaka-u.jpn.org/en/index.html), Labour and Welfare, Health and Labour Sciences Research Grant (H23-002, http://jsps-osaka-u.jpn.org/en/index.html), and from New Energy and Industrial Technology Development Organization (P10004, http://www.nedo.go.jp/english/index.html). The funders had no role in study design, data collection and analysis, decision to publish, or preparation of the manuscript.

Competing Interests: The authors have read the journal's policy and have the following conflicts: Y. Sakai was an employee of Ono Pharmaceutical Co. Ltd., and a holder of the patent for ONO-1301 encapsulated in PLGA microspheres (patent numbers WO 2004/032965 and WO 2008/047863). There are no other patents, products in development, or modified products to declare. The other authors have declared that no competing interests exist. This does not alter the authors' adherence to all PLOS ONE policies on sharing data and materials.

* E-mail: sawa@surg1.med.osaka-u.ac.jp

Introduction

Despite a number of medical and interventional treatments have been developed to treat acute myocardial infarction (AMI), the treatment for massive AMI has not been fully established. Myocardial infarction (MI) is a progressive disease, characterized by massive ischemic necrosis of the myocardial tissue and subsequent inflammation. This leads to cardiac remodeling that exacerbates the oxygen shortage in the surviving cardiac tissue. These pathological and functional deteriorations eventually cause end-stage heart failure. To delay the progression of heart failure, it is essential to suppress inflammation and fibrosis and to improve bloodflow supply in the injured myocardium consecutively. Recently, stromal cell-derived factor (SDF)-1 and its corresponding receptor CXCR4 have been shown to play prominent roles in homing of bone marrow cells (BMC) which promotes neovascularization and prevention of apoptosis via paracrine mechanism [1,2,3,4].

ONO-1301 (({5-[2-({[(1E)-phenyl(pyridin-3-yl)methylene]amino}oxy)ethyl]-7,8-dihydronaphthalen-1-yl}oxy)acetic acid) is a synthetic prostacyclin agonist. As it lacks the typical prostanoid

structure of a five-membered ring and an allylic alchol, ONO-1301 is chemically and biologically stable *in vivo*. In addition, thromboxane A2 synthethase is inhibited by ONO-1301, resulting in the promotion of endogenous prostacyclin synthesis. ONO-1301 has been reported to induce the production of endogenous hepatocyte growth factor (HGF) and vascular-endothelial growth factor (VEGF) in fibroblasts by stimulating cAMP production [5,6,7,8]. The administration of a slow-release form of ONO-1301 shows therapeutic potential, mainly due to the restoration of bloodflow in MI models of rat and swine and in a cardiomyopathic hamster [6,7,8]. The potential mechanism of the functional benefits of ONO-1301 mainly result from the enhanced secretion of growth factors, such as HGF and VEGF, which induce angiogenesis, restore bloodflow, and attenuate the progression of fibrosis. Recently we identified that ONO-1301 also upregulates SDF-1 secretion in the fibroblasts. Enhanced BMC homing in the MI heart by ONO-1301 therapy is attractive therapeutic modality. We thus hypothesized that ONO-1301 can induce BMC accumulation mediated by the upregulation of SDF-1 to elicit functional improvement in a mouse model of MI.

Methods

This study was carried out in strict accordance with the recommendations in the Guide for the Care and Use of Laboratory Animals of the National Institutes of Health. The protocol was approved by the Committee on the Ethics of Animal Experiments of the Osaka University (H23–123). All surgery was performed under sodium pentobarbital or isoflurane anesthesia, and all efforts were made to minimize suffering.

ONO-1301 and a slow-release form of ONO-1301 were purchased from ONO Pharmaceutical Co. Ltd. (Osaka, Japan) [7,8,9].

Migration Assay

Normal human dermal fibroblasts (NHDFs; Takara bio, Shiga, Japan) were cultured with or without ONO-1301 for 72 hours. The SDF-1 concentration in the culture supernatants was measured by ELISA (R&D systems, MN). BMCs were obtained from a green fluorescent protein (GFP)-transgenic mouse [C57BL/6-Tg(CAG-EGFP); Japan SLC, Inc., Shizuoka, Japan], and their migration toward the supernatants was assessed using a culture insert system (BD Falcon). The number of migrated BMCs was determined using fluorescence microscopy (Carl Zeiss, Göttingen, Germany).

Mouse AMI Model and Sheet Transplantation

An AMI model was generated by permanent ligation of the left anterior descending artery (LAD) in 10-15-week-old male C57BL/6N, BALB/cA, or BM-GFP chimera mice [10]. ONO-1301 microspheres and control microspheres were resuspended in saline at 10 mg/ml and added to atelocollagen sheets just before transplantation. Five minutes after the LAD ligation, atelocollagen sheets that included ONO-1301-containing microspheres (ONO-1301-treated group, n = 40) or empty microspheres (vehicle group, n = 40) were fixed onto the surface of the anterior left ventricular (LV) wall. The mice were euthanized 7, 21, and 28 days after the LAD ligation and ONO-1301 administration.

Assessment of BMC Homing

BMCs harvested from BALB/cA mice were labeled by Xenolight DiR (Caliper Life Sciences, MA) following the manufacturer's instructions and injected into the tail vein of BALB/cA mice after the MI and ONO-1301 treatment. On days 1 and 3, the whole-body imaging of the mice was measured by an *in vivo* imaging system (IVIS, Caliper Life Sciences).

Assessment of Cardiac Function and Survival

Cardiac function was assessed using an echocardiography system equipped with a 12-MHz transducer (GE Healthcare, WI) 4 weeks after MI and ONO-1301 treatment. The LV areas were measured, and LV fractional area change (FAC) was calculated as (LVEDA-LVESA)/LVEDA×100, where LVEDA and LVESA are the LV end-diastolic and end-systolic area, respectively.[10] The mice were housed in a temperature-controlled incubator for 28 days post-treatment to determine their survival.

Histological Analysis

Frozen sections (8 μm) of hearts were stained with antibodies against von Willebrand factor (vWF; Dako, Glostrup, Denmark) and CD31 (Abcam, UK). The secondary antibody was Alexa 546 goat anti-rabbit (Life Technologies, CA). Counterstaining was performed with 6-diamidino-2-phenylindole (DAPI; Life Technologies). The sections were also stained with isolectin (Life Technologies) following the manufacturer's instructions. To count GFP-positive cells, isolectin-positive cells, and CD31-positive capillary densities, 10 images were captured for each specimen. Capture and analysis were performed using Biorevo (Keyence, Japan). To analyze the myocardial collagen accumulation, heart sections were stained with Masson's trichrome. The collagen volume fraction in the peri-infarct area was calculated.

Quantitative Real-time PCR

The total RNA was isolated from the peri-infarct area using the RNeasy Mini Kit and reverse transcribed using Omniscript Reverse transcriptase (Qiagen, Hilden, Germany). Quantitative PCR was performed with a PCR System (Life Technologies). The expression of each mRNA was normalized to that of glyceraldehyde-3-phosphate dehydrogenase (GAPDH). The primers and probes are shown in Table S1 in File S1.

Statistical Analysis

Data are expressed as the mean ± SEM. The data distributions were checked for normality. Comparisons between 2 groups were made using the Student's *t*-test. For comparisons among 3 or more groups, one-way analysis of variance (ANOVA) followed by Fisher's protected least significant difference (PLSD) test were used. The survival curves were prepared using the Kaplan-Meier method and compared using the log-rank test. All *P*-values are two-sided, and values of $P<0.05$ were considered to indicate statistical significance. Statistical analyses were performed using the StatView 5.0 Program (Abacus Concepts, Berkeley, CA) and Statcel2 (The Publisher OMS Ltd., Saitama, Japan).

An expanded Methods section can be found in the online-only in File S1.

Results

ONO-1301 Enhanced BMC Migration via SDF-1/CXCR4 Signaling

The effect of ONO-1301 on the SDF-1 secretion by NHDFs was evaluated by ELISA. As shown in Fig. 1A, the SDF-1 concentration in the NHDF culture supernatants increased in an ONO-1301 concentration-dependent manner. The SDF-1 concentration in the culture supernatant of 1000 nM ONO-1301-treated cells was significantly greater than that of cells cultured in

the absence of ONO-1301 (Fig. 1A). To investigate the BMC migration toward ONO-1301-treated NHDF conditioned medium, a migration assay was performed using a modified Boyden chamber with 8-μm pores. The number of migrated BMCs was significantly greater in the conditioned medium of cells treated with 100 and 1000 nM ONO-1301 compared to that of cells treated with 0 and 10 nM ONO-1301. The BMC migration to the 1000 nM ONO-1301 conditioned medium was diminished by treating the BMCs with a CXCR4-neutralizing antibody or CXCR4 antagonist (AMD3100) (Fig. 1B, C).

SDF-1-mediated BMC Accumulation in the ONO-1301-treated Infarcted Hearts

The effect of ONO-1301 on SDF-1 expression in the infarcted hearts was evaluated by quantitative RT-PCR. Twenty-eight days after treatment, the SDF-1 expression in the border area of the ONO-1301-treated heart was significantly greater than that in the vehicle-treated heart (Fig. 2A). The HGF and VEGF expressions were also increased by ONO-1301 treatment (Fig. 2B, C). After LAD occlusion, ONO-1301 treatment, and intravenous injection of labeled BMCs, the BMC accumulation in the infarcted heart was evaluated by an in vivo imaging system. The proportion of BMCs in the heart showed a trend toward upregulation, dependent on the dose of ONO-1301 (Fig. 2D). Hearts treated with 100 mg ONO-1301/kg body weight showed significantly more accumulated BMCs than those treated with 0 or 10 mg ONO-1301. In 100 mg/kg ONO-1301-treated hearts, CXCR4 antagonization significantly decreased the BMC accumulation (Fig. 2D). To identify the recruited BMCs *in vivo*, the acute MI model was prepared using chimera mice by transplanting GFP-expressing bone marrow into irradiated C57BL/6 mice. The BMCs of the C57BL/6 transplant recipients were largely replaced by GFP-expressing BMCs (91.8+/−4.3%, figure S1 in File S1). The single-organ analyses using GFP-BM chimera mouse at day 7 also showed increased BMC accumulation in the ONO-1301-treated myocardium (figure S2 in File S1).

Differentiation of BMCs in the Infarcted Myocardium

Seven days after MI and ONO-1301 administration to BM-GFP chimera mouse, BMCs were dramatically accumulated in both the infarcted area and the atelocollagen sheet (Fig. 3A, B). Some of the BMCs formed tube-like structures and displayed von Willebrand factor expression (Fig. 3C, D). Isolectin staining showed that a greater percentage of isolectin-positive BMCs accumulated in the myocardium in the ONO-1301-treated (O) group than in the vehicle (V) group (Fig. 3E, F). We also evaluated small blood vessels by CD31 immunostaining. The density of small vessels was greater in the O group than in the V group (Fig. 3G). Immunohistochemical analysis of Connexin 43 and smooth muscle actin, cardiac-lineage and cardiac fibroblast markers, respectively, was also conducted at 3 months, but no co-expression

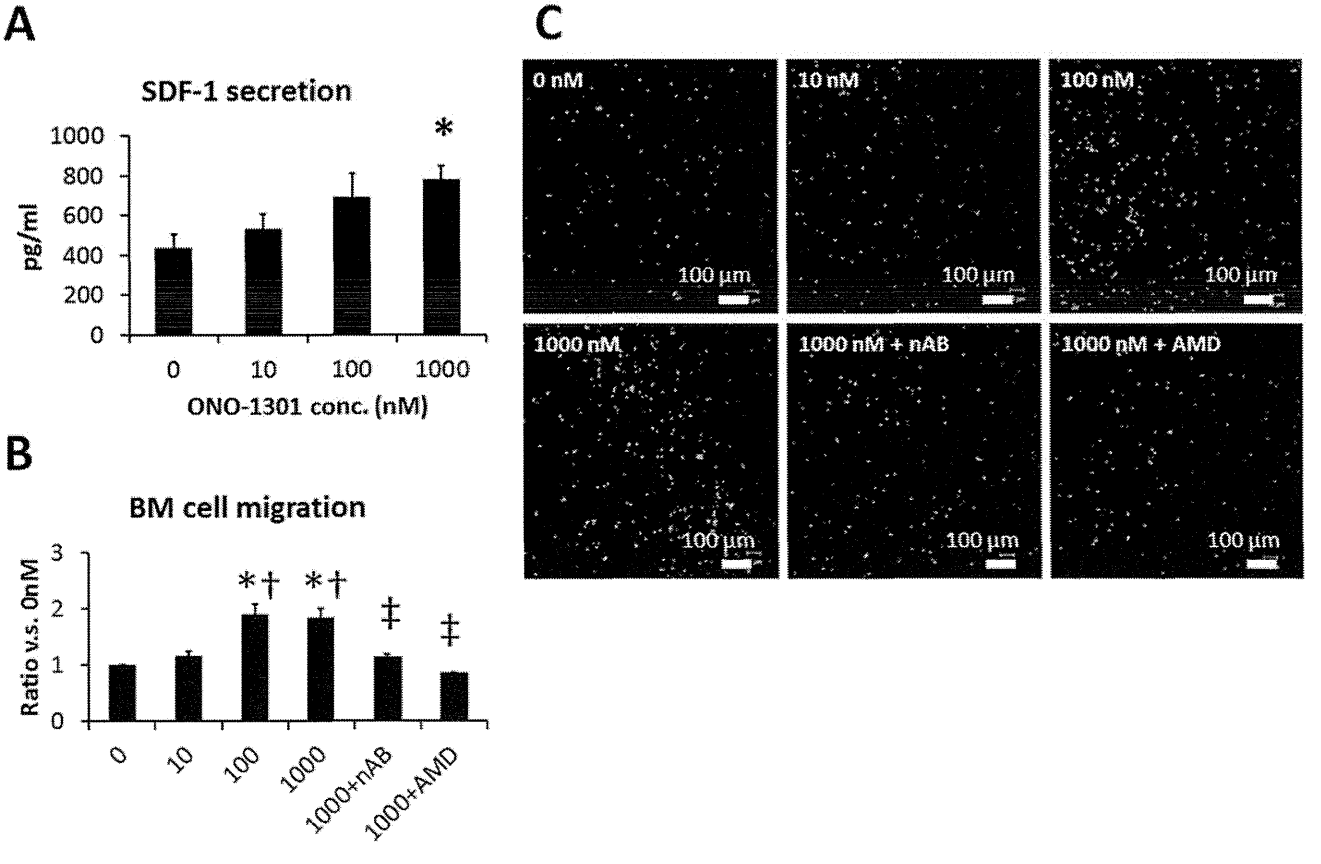

Figure 1. ONO-1301 enhanced SDF-1 secretion and BMC migration via SDF-1/CXCR4 signaling *in vitro*. NHDFs were stimulated with ONO-1301 for 72 hours, then the SDF-1 concentration in the culture medium was determined by ELISA (n = 3 each, *$P<0.05$ vs. 0 nM). A) Number of BMCs that migrated toward the conditioned medium from ONO-1301-stimulated-NHDFs (0, 10, 100, or 1000 nM ONO-1301, n = 6; 1000 nM+nAB or 1000 nM+AMD, n = 3). *$P<0.05$ vs. 0 nM, †$P<0.05$ vs. 10 nM, ‡$P<0.05$ vs. 1000 nM, §$P<0.05$ vs. SDF-1. nAB, CXCR4-neutralizing antibody; AMD, CXCR4 antagonist AMD3100. B) Representative pictures of BMCs that had migrated to the medium from ONO-1301-stimulated BMCs. Green, BMCs.
doi:10.1371/journal.pone.0069302.g001

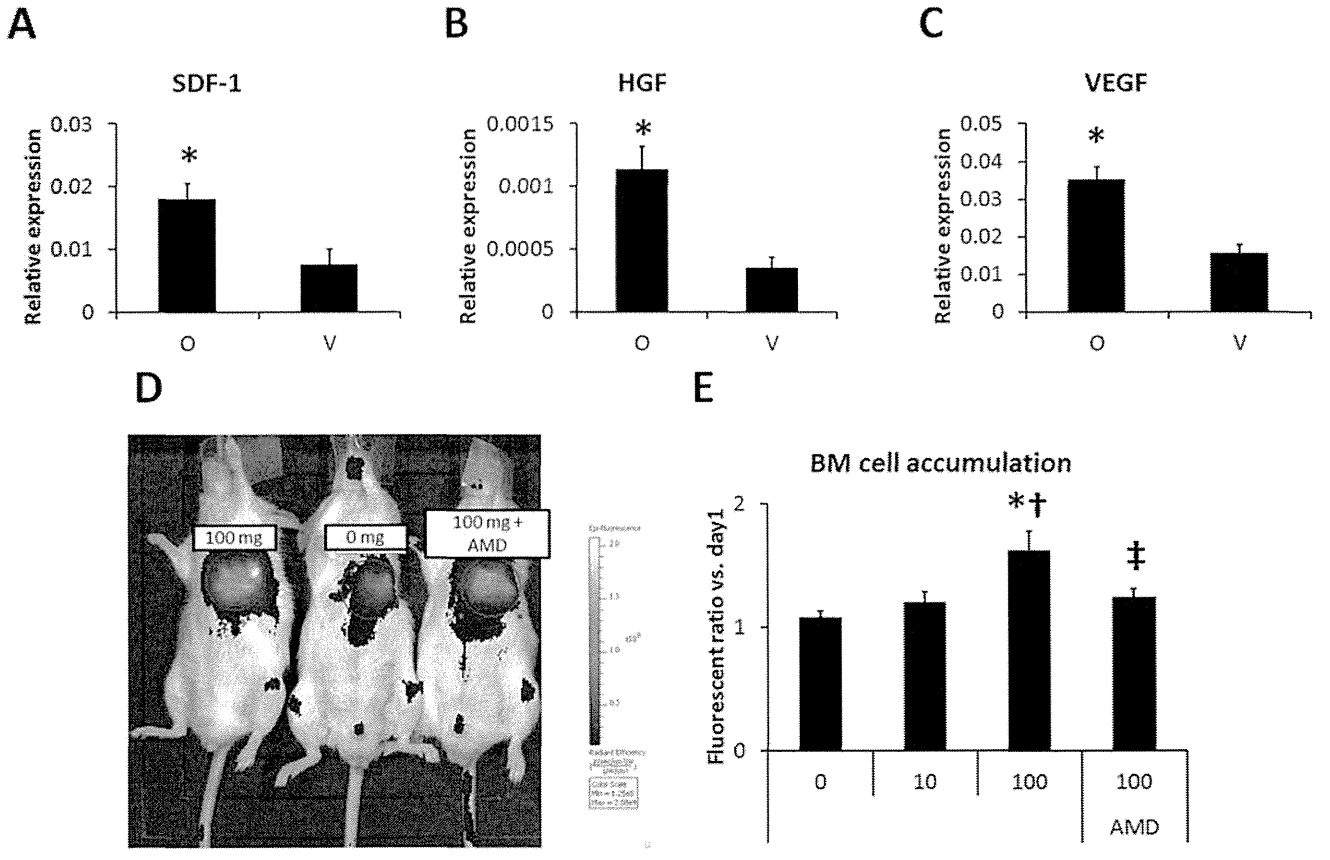

Figure 2. ONO-1301 enhanced SDF-1 secretion and BMC migration via SDF-1/CXCR4 signaling after MI. A–C) The SDF-1, HGF, and VEGF expression at the border zone of the infarcted area was measured by quantitative RT-PCR. The expression levels of these cytokines were higher in the ONO-1301-treated (O) group compared to the vehicle (V) group. (O group, n = 7; V group, n = 7–8; *$P<0.05$ vs. V group). The expression relative to GAPDH is shown. D) BMC migration to ONO-1301-treated infarcted myocardium was evaluated using IVIS. Representative picture of IVIS at day 3. Left: 100 mg/Kg, Center: 0 mg/Kg, Right: 100 mg/Kg+AMD3100 (AMD). E) The number of accumulated BMCs was greater in the 100 mg/kg ONO-1301-treated infarcted heart compared to the 0 and 10 mg/kg ONO-1301-treated infarcted heart. When BMCs treated with AMD were injected, the BMC accumulation decreased in the 100 mg/Kg ONO-1301-treated infarcted heart compared with the untreated-BMC-injected heart (0 mg/Kg, n = 4; 10 mg/Kg, n = 8; 100 mg/Kg, n = 5; 100 mg/Kg+AMD3100, n = 4; *$P<0.05$ vs. 0 mg/Kg, †$P<0.05$ vs. 10 mg/Kg, ‡$P<0.05$ vs. 100 mg/Kg).
doi:10.1371/journal.pone.0069302.g002

of GFP with either of these markers was observed (figure S3 in File S1).

Therapeutic Effects of ONO-1301 Administration on Cardiac Performance, Survival, and LV-remodeling at 4 Weeks Post-MI

ONO-1301 was detected in the plasma of blood samples from the ONO-1301-treated group 3 weeks after treatment (figure S4 in File S1). The cardiac functions in the MI mice with and without following ONO-1301 treatment were evaluated. Mortality was substantial until 14 days post-LAD ligation in the vehicle group, and similar mortality levels were observed with non-treated MI mice [11]. In contrast, in the ONO-1301-treated group, there was little mortality 7 days after MI, and thus a difference in survival (Fig. 4A). Cardiac performance was evaluated by 2D echocardiography 4 weeks after implantation. The LVEDA was smaller in the ONO-1301-treated group than in the vehicle group, but the difference was not significant. In contrast, the LVESA was significantly smaller, and the LVFAC was significantly greater, in the ONO-1301-treated group than in the vehicle group (Fig. 4B). In the histological analysis, the vehicle group showed a typical MI with a large anterior LV scar and dilatation of the LV cavity. By comparison, the LV of the ONO-1301-treated group was less dilated, and the anterior wall was thicker (Fig. 4C, D). The infarcted area and percent fibrosis were significantly smaller in the ONO-1301-treated than in the vehicle-treated group (Fig. 4C, E–G).

Discussion

Here, we showed that ONO-1301 promotes BMC accumulation in the injured myocardium. *In vitro*, ONO-1301 enhanced SDF-1 expression, and BMC migration was greater to conditioned medium obtained from ONO-1301-stimulated cells. The enhanced migration was diminished by blocking SDF-1/CXCR4 signaling. Consistent with the *in vitro* experiments, ONO-1301 enhanced the SDF-1 expression of myocardial tissue. High ONO-1301 accelerated the BMC accumulation after MI in a SDF-1/CXCR4-dependent manner. Some BMCs in the infarcted myocardium differentiated into capillary structures within 7 days. Furthermore, the sustained-release delivery of ONO-1301 in the infarcted myocardium also led to functional improvements following MI. Our data suggest that ONO-1301 is a novel inducer of BMC recruitment, and that ONO-1301 treatment may be a promising therapeutic strategy for the clinical treatment of MI.